Journal of Statistical Physics, Vol. 35, Nos. 5/6, 1984

Dynamics of the Formation of Two-Dimensional Ordered Structures

A. Sadiq[1,2] **and K. Binder**[1,3]

Received November 1, 1983

The growth of ordered domains in lattice gas models, which occurs after the system is quenched from infinite temperature to a state below the critical temperature T_c, is studied by Monte Carlo simulation. For a square lattice with repulsion between nearest and next-nearest neighbors, which in equilibrium exhibits fourfold degenerate (2×1) superstructures, the time-dependent energy $E(t)$, domain size $L(t)$, and structure function $S(q, t)$ are obtained, both for Glauber dynamics (no conservation law) and the case with conserved density (Kawasaki dynamics). At late times the energy excess and halfwidth of the structure factor decrease proportional to t^{-x}, while $L(t) \propto t^x$, where the exponent $x = 1/2$ for Glauber dynamics and $x \approx 1/3$ for Kawasaki dynamics. In addition, the structure factor satisfies a scaling law $S(k, t) = t^{2x}\tilde{S}(kt^x)$. The smaller exponent for the conserved density case is traced back to the excess density contained in the walls between ordered domains which must be redistributed during growth. Quenches to $T > T_c$, $T = T_c$ (where we estimate dynamic critical exponents) and $T = 0$ are also considered. In the latter case, the system becomes frozen in a glasslike domain pattern far from equilibrium when using Kawasaki dynamics. The generalization of our results to other lattices and structures also is briefly discussed.

KEY WORDS: Domain growth; Glauber and Kawasaki model; dynamic scaling; Monte Carlo simulation; lattice gas model.

[1] Institut für Festkörperforschung der Kernforschungsanlage Jülich, Postfach 1913, D-5170 Jülich, West Germany.

[2] Alexander von Humboldt Fellow. Permanent and present address: Pakistan Institute of Nuclear Science and Technology, P.O. Nilore, Rawalpindi, Pakistan.

[3] Address after October 1, 1983: Institut für Physik, Universitaet Mainz, D-6500 Mainz, West Germany.

0022-4715/84/0600-0517$03.50/0

1. INTRODUCTION AND REVIEW OF THE PROBLEM

Recently there has been considerable theoretical interest in the kinetics of domain growth in systems which are quenched from high temperatures in the disordered phase to a temperature below a transition temperature of an order–disorder transition.[1–20] This is clearly a rather fundamental problem in the statistical mechanics of nonlinear phenomena far from equilibrium. In addition, this problem is of practical interest in metallurgy[21,22] and surface science.[23,24] By describing this problem in terms of the dynamics of random interfaces between domains,[1,6,15–18] the relation to problems like phase separation via nucleation and spinodal decomposition,[4] pattern formation in crystal growth,[5] and critical dynamics in low dimensions[27] can be established.

Immediately after the quench the ordered phase appears in the form of extremely small and irregular domains separated by walls, since the order parameter always has some degeneracy corresponding to the symmetry which is broken at the transition, and none of the degenerate orderings is preferred. We here assume that only a finite number p of such degenerate orderings exist, as is appropriate for lattice gas models with superstructures commensurate with the lattice. For example, $p = 2$ for the ordinary Ising antiferromagnet, but we shall be mainly interested in orderings with $p > 2$; with the respect to static critical phenomena[28] such models may belong[6] to "universality classes" such as the three- or four-state Potts model[7] or the XY model with cubic anisotropy.[31] In all these systems we expect that these domains coarsen, as the time t after the quench increases, and thus the (unfavorable) excess free energy due to the walls is reduced. In the late stages, the domain sizes are much larger than all microscopic lengths. Thus there exists a loose analogy with critical phenomena, where the order parameter correlation length ξ is much larger than all microscopic lengths and as a consequence, all quantities in the critical region are described by simple power laws, satisfying scaling relations, the exponents being the same for all systems belonging to a given universality class.[28,29] Both with respect to static[28,29] and dynamic[32] critical phenomena, one understands now well which universality classes exist and has reasonably accurate estimates for the universal exponents involved. On the basis of the analogy with critical phenomena, one also expects[33] the growth law for the domain

[4] For a recent review, see Ref. 25.

[5] For a review, see Ref. 26.

[6] For a review of the classification of models into universality classes in two dimensions, see Ref. 29.

[7] For a review, see Ref. 30.

size $L(t)$, and the decay law for the internal energy excess $E(t) - E(\infty)$, etc., to have power-law form,

$$L(t) \propto t^x, \qquad E(t) - E(\infty) \propto t^{-y} \tag{1}$$

Here x, y, etc. are some "universal" exponents. Also the structure factor $S(\mathbf{q}, t)$, which is accessible in scattering experiments, can be cast in a scaled form

$$S(q,t) = \left[L(t) \right]^d \tilde{S} \left\{ kL(t) \right\} \tag{2}$$

d being the dimensionality, the wave vector $\mathbf{k}$ is measured relative to the Bragg positions of the ordered structure $\mathbf{Q}$, $\mathbf{k} = \mathbf{q} - \mathbf{Q}$, and $\tilde{S}(\zeta)$ is some scaling function. Actually Eq. (2) was first proposed[33,34] and verified[35–37] for spinodal decomposition, where $\mathbf{Q} = 0$, and later generalized to ordering kinetics.[7–10,12] Even in the case of spinodal decomposition of solids, where one thinks that $x = y = 1/3$,[39–41,34] the exponents are well established only for the regime where the growing domains of the new phase take a small volume fraction. For large volume fractions the growing domains form an interpenetrating percolation network,[42] and it is conceivable that there different exponents apply.[42,43] In addition, even for small volume fraction it is difficult to obtain an accurate description of the scaling function $\tilde{S}\{\zeta\}$.[44,45] Even much less is known about ordering kinetics, however: the possible universality classes and their exponents and scaling functions have not yet been sorted out. Only for the case of twofold degenerate ordering ($p = 2$), all theories agree that $x = y = 1/2$,[1–20] and it makes no difference whether a quantity other than the order parameter (such as the density, for instance) is conserved. Even in this case, however, there are still serious problems in understanding dependences on parameters such as temperature.[18,20] Even much less is known for orderings with larger order parameter degeneracy p. Larger p are of great physical interest; they occur for ordered monolayers at surfaces (e.g., $p = 3$ for the $\sqrt{3} \times \sqrt{3}$ structure on triangular lattices, 3×1 structure on rectangular lattices; $p = 4$ for the 2×2 structure on square and triangular lattices, 2×1 structure on square lattices, 4×1 structure on rectangular lattices; see e.g., Ref. 29) and for ordered binary alloys (e.g., the CuAu ordering on the fcc lattice has $p = 3$, while the Cu_3Au ordering has $p = 4$; see e.g., Ref. 46 for model phase diagrams). It was pointed out that for $p > d + 1$ one could have locked-in domain configurations, which would result in a domain growth law as slow as $L(t) \propto \ln t$.[11] It is now realized that such a locking in of the domain configuration at nonzero temperature can hardly occur, and thus this law is not observed.[16,17,47] Recent simulations of the p-state Potts model with Glauber dynamics yielded[17] $x = 1/2$ for $p \lesssim 6$, while for $6 \lesssim p \lesssim 26$ the

exponent seemed to decrease continuously with increasing p, and reached a limiting value $p \approx 0.41$ for larger p. The limit $p \to \infty$ might be physically applicable to the growth problem of crystalline grains in metals.[17] A theoretical understanding of this p dependence of the growth law exponent x so far is lacking. Very recently it was suggested[48] that a chaotic interplay of several growth mechanisms, which compete with each other irrespective of the domain length scale $L(t)$, might lead to an intermittency effect (like in fully turbulent fluid flow) and then decrease the exponent x from $1/2$ to a nonuniversal smaller value.

In the present paper we contribute to this interesting problem of sorting out the universality classes of domain growth by presenting and analyzing Monte Carlo simulations of additional models. We concentrate on a lattice gas model on the square lattice with repulsive interactions between nearest and next-nearest neighbor interactions of equal strength. For densities $\rho = 1/2$ or near that value, this model undergoes a second-order transition to the (2×1) structure[49] (while for densities around $\rho \approx 1/4, 3/4$ the phase diagram still is controversial.[49-52]) This structure has $p = 4$, but it does not belong to the four-state Potts universality class, with respect to critical phenomena, but to the class of the XY model with cubic anisotropy.[31] Thus comparing our results with the four-state Potts results of Ref. 17 has bearing on the question whether the domain growth universality classes are uniquely specified by p already, or depend on other symmetry properties as well. Secondly, we shall conduct a comparative study of the model using both "Glauber dynamics"[53,54] and "Kawasaki dynamics."[54,55] The latter conserves the density ρ while the former does not. Domain growth at conserved density corresponds to the physical situation in case of chemisorbed systems, a large variety of which exist,[8] and where domain growth can indeed be observed.[24,57] While the $p(2 \times 1)$ structure of O on W(112) studied in Ref. 24 has $p = 2$ and hence x should be $1/2$, in agreement with observation,[24] O on W(110) would be a realization of a (2×1) structure with $p = 4$,[56] for instance. "Kawasaki dynamics"[54,55] then models surface diffusion events.[9] On the other hand, the simulations using "Glauber dynamics" correspond to physisorbed monolayers (such as monolayers on grafoil[29]), which are in thermal equilibrium with a surrounding gas. Glauber dynamics[53,54] then simulates the random evaporation and condensation events of adsorbate atoms on the surface.

We emphasize this distinction between the conserved and nonconserved case, because we find, in contrast to the case $p = 2$, that they belong

[8] For a review on chemisorbed monolayers, undergoing order–disorder transitions, see Ref. 56.
[9] See also Ref. 58 for a detailed study of surface diffusion in the present model.

to different universality classes of domain growth for larger p.[10] The importance of density conservation for $p \geqslant 3$ will be linked to the excess density contained in the walls between the various possible ordered domains.

In Section 2, we give a description of our methods, and describe also their application to quenches which lead to a final state above T_c in the one-phase region. In such a case, the approach to equilibrium is much easier to understand theoretically, and hence the simulation of this problem serves as an accuracy check of our methods. Particular attention will be paid to finite size effects. Section 3 then describes our numerical results for quenches to $T < T_c$ with "Glauber dynamics" and Section 4 the results for quenches with "Kawasaki dynamics." Section 5 is devoted to quenches which lead to $T = 0$, where with Kawasaki dynamics a frozen-in glasslike domain pattern is found. Section 6 is devoted to quenches leading to T near T_c and contains a discussion of the observed critical behavior. Section 7 then discusses the problem of excess density in domain walls for several other structures and lattices, in order to show that our findings are not restricted to the particular model which was investigated in detail. Section 8 then contains our conclusions.

2. SIMULATION TECHNIQUES AND THEIR APPLICATION IN THE DISORDERED REGION

We consider a square lattice of linear dimensions $\sqrt{N} \times \sqrt{N}$ and periodic boundary conditions. In "magnetic terminology," the Hamiltonian is given by

$$\mathscr{H} = -J_{\mathrm{nn}} \underbrace{\sum_{\langle i,j \rangle}}_{\text{nearest neighbors}} S_i S_j - J_{\mathrm{nnn}} \underbrace{\sum_{\langle i,j \rangle}}_{\text{next nearest neighbors}} - H \sum_{i=1} S_i ,$$

$$S_i = \pm 1 \quad (3)$$

where J_{nn}, J_{nnn} are interaction parameters between nearest and next-nearest neighbors, H is a magnetic field, and the sums $\langle i, j \rangle$ run over all pairs i, j once. In most of our simulations, we choose $J_{\mathrm{nn}} = J_{\mathrm{nnn}}$ and the units of temperature such that $|J_{\mathrm{nn}}| = 1$. As is well known, Eq. (3) is equivalent to a lattice gas where each site can either be occupied ($c_i = 1$) or empty ($c_i = 0$), using $S_i = 1 - 2c_i$, which yields (omitting an unimportant constant)

$$\mathscr{H} = \mu N_a = -\phi_{\mathrm{nn}} \underbrace{\sum_{\langle i,j \rangle}}_{\text{nearest neighbors}} c_i c_j - \phi_{\mathrm{nnn}} \underbrace{\sum_{\langle i,j \rangle}}_{\text{next nearest neighbors}} c_i c_j \quad (4)$$

[10] A very brief and preliminary account of these results was also given in Ref. 59.

where $N_a = \sum_{i=1}^{N} c_i = N\rho$ is the number of occupied sites of the lattice (ρ being the density when we measure all lengths in units of the lattice spacing). The chemical potential in Eq. (4) is in our case

$$\mu = -8J_{nn} - 2H \tag{5}$$

and the interaction parameters $\phi_{\mathrm{nn}}, \phi_{\mathrm{nnn}}$ are simply given as $\phi_{\mathrm{nn}} = 4J_{\mathrm{nn}}$, $\phi_{\mathrm{nnn}} = 4J_{\mathrm{nnn}}$.

This model undergoes a second-order transition to a (2×1) structure, at a critical temperature (for $H = 0$ or equivalently, $\rho = 1/2$) of about $T_c \approx 2.1$. Figure 1 shows the four types of ordered domains which are possible in this model. In lattice gas terminology, the ordering consists of a succession of alternating full and empty rows. The order is fourfold degenerate, because full and empty rows may be interchanged (a, b), and they may also be oriented along the y axis (c, d) rather than along the x axis.

Our simulations always start with either a random spin configuration (Glauber dynamics) or a randomly occupied lattice gas configuration consistent with a given density ρ. Thus we always start from infinite temperature, although it would be a rather straightforward extension to first let the system equilibrate at some finite (high) temperature, if one wishes to consider quenches from that temperature. In the case of Glauber dynamics, we randomly select a spin, S; and flip it if its transition probability[53]

$$\tau W(S_i \to -S_i) = \tfrac{1}{2}\left[1 - \tanh(\delta\mathscr{H}/T)\right] \tag{6}$$

exceeds a random number ζ chosen uniformly from the interval $[0, 1]$. In Eq. (4), τ is an arbitrary factor setting a time scale, such that $W(S_i \to -S_i)$

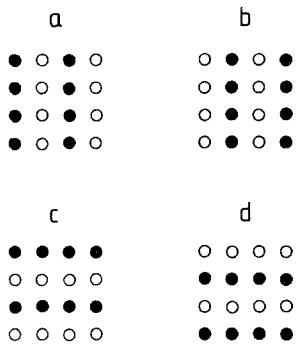

Fig. 1. Four ordered ground state configurations (denoted by a, b, c, d) of the square lattice with nearest and next-nearest neighbor repulsive interaction. Occupied sites ("spin down") are indicated by full circles, empty sites ("spin up") by empty circles. This order is denoted as (2×1) structure.

is a transition probability per unit time for the spin flip, and $\delta\mathscr{H}$ is the energy change involved in the flip. T is the temperature to which we quench. As is well known,[54] Eq. (4) satisfies a detailed balance condition with the thermal equilibrium probability of a spin configuration $P_0(\{S_i\}) \propto \exp(-\mathscr{H}\{S_j\}/T)$, and the approach toward equilibrium is described by a master equation for the probability $P(\{S_j\}, t)$ that the configuration $\{S_j\}$ occurs at time t,

$$\frac{d}{dt}P(\{S_j\},t) = -\sum_i W(S_i \to -S_i)P(\{S_j\},t) + \sum W(-S_i \to S_i)P(\{S_{j\neq i}, -S_i\},t) \tag{7}$$

Here the time t is proportional to the sequential label of configurations $\{S_j\}_\nu$ generated, $t = \nu/N$ if we measure time in units of attempted flips per spin, choosing also the time constant τ equal to unity. The zero of time corresponds to the instant where the quench is performed (in a real experiment this would mean an infinitely high cooling velocity). Similarly, in the case of Kawasaki dynamics we randomly select an *occupied* site i and a nearest-neighbor site l_i of it. Then the chosen particle is moved to the site l_i according to the transition probability[58]

$$\tau W(c_i \to c_{l_i}) = \tfrac{1}{2}(1 - c_{l_i})\left[1 - \tanh(\delta\mathscr{H}/T)\right] \tag{8}$$

Here the factor $(1 - c_{l_i})$ ensures that particles can only jump to neighboring empty sites. Owing to this factor, Eq. (8) differs from Kawasaki's original model where also parallel spins can be exchanged.[55] Time is then measured in units of attempted jumps per particle.

If one considers quenches to very low temperature, after a short transient period almost all attempted spin flips (or particle jumps, respectively) would involve an energy cost $\delta\mathscr{H} > 0$, and since then $\delta\mathscr{H}/T \gg 1$, are almost always unsuccessful since the transition probability is so small. This inefficiency is particularly cumbersome for the "Kawasaki dynamics," since energy changes typically are nearly a factor two larger than for "Glauber dynamics." Thus a more efficient algorithm has been developed,[60] which extends the so-called "n-fold way," developed by Bortz *et al.*[61] for Glauber dynamics, to Kawasaki's dynamics. This algorithm samples preferentially the "active bonds," which have $\delta\mathscr{H} < 0$, by selecting particle-hole pairs not completely at random but with a probability proportional to their transition probability. Thus every move is successful, but the time increment after each move is different and has to be computed from the algorithm itself. But is has been shown and carefully tested, that with the appropriately rescaled time one obtains physical results from this algorithm which are identical with the ordinary algorithm. While this new

algorithm in the late stages of a domain growth simulation typically performs one or two orders of magnitude faster than the standard code, the situation actually is reverse in the initial stages, where anyhow a larger fraction of particle moves has $\delta\mathscr{H} < 0$. Thus simulations at quenches to very low temperature were performed in a sort of "hybrid algorithm," which was the standard one up to a time between $t = 1000$–3000 MCS (1 MCS = 1 Monte Carlo step per particle), and then the program switched to the new algorithm. More details can be found in Ref. 60.

Lattice sizes used were in the range 40×40 up to 800×800, in order to watch out for finite size effects; the bulk of our calculations were performed for lattice sizes 80×80 or 120×120, respectively. There are several ways in which finite size limits the accuracy of the simulation:

(i) The correlation length of order parameter fluctuations in an equilibrium state is large. This occurs only for quenches very close to T_c, and will not be important for the numerical data presented below.

(ii) The average domain size $L(t)$ after some time t is large.

Both for quenches to $T = T_c$ and for quenches to $T < T_c$ ($T > 0$ for "Kawasaki dynamics") we expect $L(t) \to \infty$ in the thermodynamic limit. Hence only such times t were considered where $L(t) \ll \sqrt{N}$ [in practice we stopped at $L(t) \approx \sqrt{N}/4$.]

(iii) As there are only four kinds of domains present the volume fractions of which will fluctuate, in the late stages there is the possibility that the kind of domains whose volume fraction has a distinct majority may start to form a percolating object (extending in one or both lattice directions over the entire lattice). If this occurs, it surely affects the domain growth rates. While we found evidence for this domain percolation rather frequently, when $L(t) \gtrsim \sqrt{N}/2$, it occurred only very rarely for $L(t) \lesssim \sqrt{N}/4$. We expect this problem to be more serious for the case of three dimensions, where percolation phenomena occur at much lower volume fractions than in two dimensions.[62]

(iv) Owing to the periodic boundary conditions, wavevectors $\mathbf{q}$ in the structure factor $S(\mathbf{q}, t)$ can not occur in a continuum, but only for discrete values.

$$\mathbf{q} \equiv \{q_x, q_y\} = \frac{\pi}{\sqrt{N}} \{\nu_x, \nu_y\} \tag{9}$$

with ν_x, ν_y integers in the range $-\sqrt{N} < \nu_x, \nu_y \leqslant \sqrt{N}$. As a result not only the structure factor $S(\mathbf{q}, t)$ of an infinite system is inaccurately represented, particularly if $L(t) \gg 1$, but also mode-coupling effects due to the conservation law for the density in the case of "Kawasaki dynamics" will be affected, since the conservation law leads to "hydrodynamic slowing down"[63,54] for $\mathbf{q} \to 0$, but this slowing down is rounded off at the smallest

wavevector $|q| = \pi/\sqrt{N}$. We shall study this phenomenon in more detail for $T > T_c$ below.

(v) In a finite system, the energy per spin E will show spontaneous stochastic fluctuations in thermal equilibrium; the mean-square amplitude of these fluctuations is given by the fluctuation relation $\langle E^2 \rangle - \langle E \rangle^2 = T^2 C/N$, C being the specific heat per spin in equilibrium. Consequently, when we study the decay of the energy excess $E(t) - \langle E \rangle$ in a quench, we are limited to times where this excess exceeds the level of statistical fluctuations distinctly, if we use a single quenching run. It turns out that for the system sizes used this hardly would be satisfactory, and hence it turns out necessary to average the results over many quenching runs, using different (but equivalent) initial conditions for each. Typically, we average over the order of 10^2 samples, while for the 400×400 system we generated four samples only; and for the 800×800 system we used a single run. Since one large system is equivalent to a large number of smaller subsystems, the statistical accuracy of the energy relaxation is automatically better for the large system. Somewhat surprisingly, we did not confirm this averaging property for quantities growing in time, such as the average domain size $L(t)$: one run for the 800×800 system is, particularly in the initial stages, significantly noisier than the average of 100 systems taken for the size 80×80, although this involves precisely the same number of total spins (see Fig. 15 below). We feel that this is due to the fact that fluctuations present in the initial state are also amplified during a transient period of time, as the initially homogeneous state at the temperature to which the quench leads is highly unstable. Thus the level of such fluctuations, which are then seen as fluctuations in $L(t)$, reaches a much larger value than one would predict from the above statistical considerations. The transient amplification of fluctuations around a state evolving in time so far has been considered only in the context of spinodal decomposition.[64]

We now return to problem (iv), discussing the relaxation of energy in the regime of the disordered phase. With no conservation law, i.e., Glauber dynamics, the energy after an initial transient period, where the relaxation is governed by nonlinear effects, must relax exponentially fast toward equilibrium. This "linear regime" where the equilibrium relaxation time dominates, should near T_c only be reached, however, when $E(t) - \langle E \rangle \propto |1 - T/T_c|^{1-\alpha}$, where α is the specific heat exponent and the proportionality constant is of order unity.[65,66] In order to be able to see both the nonlinear and linear regimes in the energy relaxation, we hence have chosen $T = 2.5$ which exceeds T_c by about 20%. Figure 2 shows the results of such simulations of relaxation for both Glauber and Kawasaki dynamics. In fact, while the relaxation in the Glauber case is distinctly nonexponential for $t \lesssim 10$, the data are consistent with an exponential decay for

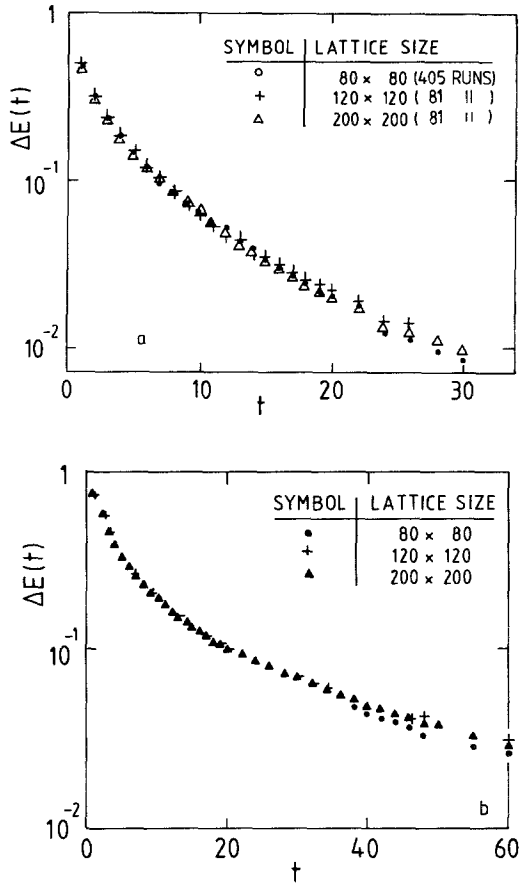

Fig. 2. (a) Relaxation of energy per spin (measured also in units of $|J_{nn}|$) plotted vs. time on the semilogarithmic scale (straight line indicates exponential decay), for Glauber single spin-flip dynamics, $H = 0$ (i.e., $\rho = 0.5$), and a quench temperature $T = 2.5$. Results for sizes 80×80, 120×120, and 200×200 have been averaged over 405, 81, and 81 runs, respectively. (b) Same as (a) but for Kawasaki spin exchange (i.e., particle hopping) dynamics.

$t \gtrsim 10$. It is quite hard to establish this asymptotic decay law precisely, however, since for $t \approx 25$ the energy excess $E(t) - \langle E \rangle$ is of the order of 10^{-2} only, and in spite of the large number of samples hampered by statistical fluctuations there already. But at least it is gratifying that there are no statistically significant finite-size effects.

The simulation data for the case with conserved density at first sight look similar (Fig. 2b). This fact is surprising since a simple argument[33] shows that one there expects a different decay law. From Eq. (4) we note

that the equilibrium energy can be written

$$\langle E \rangle = -\sum_{\mathbf{q}} \phi(\mathbf{q}) S_{\text{eq}}(\mathbf{q}) \tag{10}$$

where $\phi(\mathbf{q})$ is the Fourier transform of the interactions

$$\phi(q) = \phi_{\text{nn}} \sum_{\substack{j, \text{ nearest} \\ \text{neighbors of } i}} \exp\{-i\mathbf{q} \cdot (\mathbf{r}_i - \mathbf{r}_j)\} + \phi_{\text{nnn}} \sum_{\substack{j, \text{ next nearest} \\ \text{neighbors of } i}} \exp\{-i\mathbf{q} \cdot (\mathbf{r}_i - \mathbf{r}_j)\} \tag{11}$$

and $S_{\text{eq}}(\mathbf{q}) \equiv \langle c(-\mathbf{q}) c(\mathbf{q}) \rangle$ is the structure factor in equilibrium,

$$S_{\text{eq}}(q) = \frac{1}{N} \sum_{k,l} \exp\{iq \cdot (\mathbf{r}_k - \mathbf{r}_l)\} \langle c_k c_l \rangle \tag{12}$$

Now the conservation law of the density implies that in the limit $q \to 0$, $t \to \infty$, $q^2 t =$ finite, the structure factor approaches equilibrium exponentially with a factor $\exp(-Dq^2 t)$, D being the (collective) diffusion constant.[33,54,63] As a consequence, the relaxation of $E(t)$ will contain a term

$$E(t) - \langle E \rangle \propto \sum_{\mathbf{q}} \phi(\mathbf{q}) S_{\text{eq}}(\mathbf{q}) \exp(-Dq^2 t) \tag{13}$$

In the limit considered the q dependence of $\phi(\mathbf{q}) S_{\text{eq}}(\mathbf{q})$ can be neglected, and hence, in two dimensions

$$E(t) - \langle E \rangle \propto \phi(0) S_{\text{eq}}(0) \sum_{q} \exp(-Dq^2 t) \propto \int d\mathbf{q} \exp(-Dq^2 t) \propto t^{-1} \tag{14}$$

Additional exponentially fast decaying terms at late times always will be negligibly small in comparison with this term exhibiting power-law decay.

In order to check for this decay, we replot the data of Fig. 2 in log–log form (see Fig. 3). In the Glauber case, the data exhibit in this plot much curvature and quickly reach a slope much larger than unity. This indicates that a power-law decay is not appropriate, as expected. But in the Kawasaki case, too, although there is less curvature in the late stages one reaches a slope distinctly larger than unity, namely, about 1.2, in disagreement with the theoretical answer, Eq. (14), that the slope asymptotically should be unity.

The clue to explain this discrepancy lies in a small but systematic variation of the data with finite size, which is beyond the statistical error in Figs. 2b, 3b, in contrast to Figs. 2a, 3a. This small variation with size must here be expected because of the discreteness of $\mathbf{q}$ space: thus the step in Eq. (14) leading from $\sum_q$ to $\int d\mathbf{q}$ is not fully justified in a finite lattice. In Fig. 4 we have studied this finite-size effect, by just calculating $\sum_{\mathbf{q}} \exp(-Dq^2 t)$ for

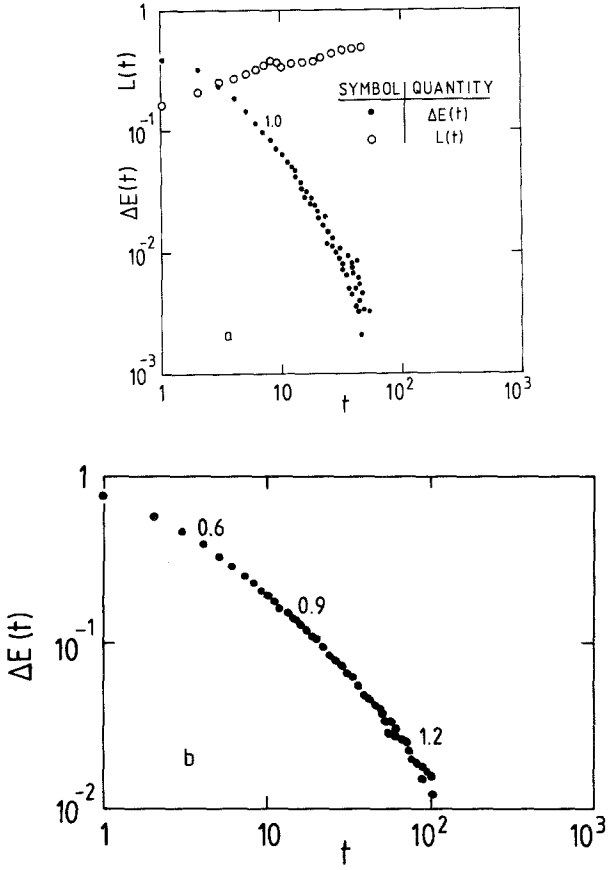

Fig. 3. Same data as Fig. 2, but replotted in log–log form, for the Glauber case (a) and Kawasaki case (b). Numbers at the curves indicate the effective exponent near that time. A "length" $L(t)$ included in case (a) is defined for $T > T_c$ from $\{N[\psi_1^2(t) + \psi_2^2(t)]\}^{1/2}$, of Eq. (15).

finite lattices summing over the allowed $\mathbf{q}$ values as specified in Eq. (9). In fact, over the first two decades of decay (i.e., on a comparable ordinate scale as Fig. 3b) one sees a pattern of behavior very similar to the simulation: there are small but systematic size effects leading to a quicker decay than occurs in the infinite system, and giving rise to a curvature which expresses crossover to an asymptotically exponential decay proportional to $\exp(-D\pi^2 t/N)$, rather than exhibiting clearly the correct t^{-1} decay law.

We have presented this example in detail because it vividly illustrates the difficulty of properly analyzing computer experiments on asymptotic decay laws (or growth laws, respectively): with somewhat less statistics, one

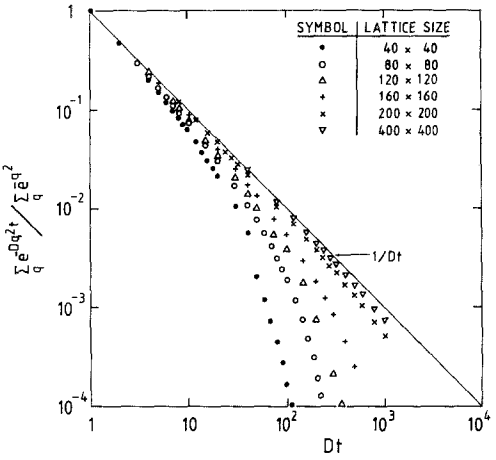

Fig. 4. Log–log plot of $\sum_q \exp(-Dq^2t)$ vs. Dt for various finite lattices.

would not be able to see any systematic size effects in Figs. 2b, 3b at all, and in the absence of knowledge what to expect one might easily conclude that the exponent of the decay is 1.2 or even larger. As a consequence, it is necessary to obtain data with very good statistical accuracy over as wide a range of lattice sizes and of times as possible, in order to draw reliable conclusions.

3. ORDERING KINETICS WITH "GLAUBER DYNAMICS"

Again a random spin configuration is used as initial state for the quench, but now we consider final temperatures T and field H such that the equilibrium would be an ordered state (Fig. 5). Only the case $H = 0$ has been studied and hence $\rho = 0.5$, and the temperatures chosen were $T = 1.33$ and $T = 0.75$ (temperatures in the critical region, $T = 2.0$, 2.1, and 2.2, respectively, will be considered in Section 6, while the case $T = 2.5$ was discussed in the previous section). Dividing the system into four sublattices corresponding to a 2×2 unit cell, the two-order parameter components ψ_1, ψ_2 of the (2×1) structure (Fig. 1) can be expressed in terms of the sublattice magnetizations m_1, m_2, m_3, m_4 as $\{m_\nu = (1/N)\sum_{i \in \nu} S_i\}$

$$\psi_1 = m_1 + m_2 - m_3 - m_4, \qquad \psi_2 = m_1 - m_2 - m_3 + m_4 \tag{15}$$

The four fully ordered possibilities of the (2×1) structure correspond simply to the cases $(\psi_1 = 1, \psi_2 = 0)$, $(\psi_1 = -1, \psi_2 = 0)$, $(\psi_1 = 0, \psi_2 = 1)$, and $(\psi_1 = 0, \psi_2 = -1)$, respectively. In the simulations of quenching, all four types of ordered states will occur and hence it is convenient to describe the degree of order by a root-mean-square order parameter $[\psi_1^2(t) + \psi_2^2(t)]^{1/2}$

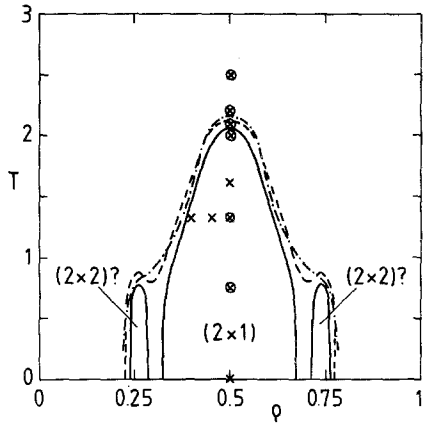

Fig. 5. Phase diagram of the Ising square lattice with nearest and next-nearest neighbor repulsion. Solid curve is the phase boundary between ordered and disordered states according to the transfer matrix calculation of Ref. 50, the dash-dotted curve the phase boundary estimated in Ref. 49 from Monte Carlo simulations on a 40×40 lattice, and the broken curve is a contour of constant correlation length $\xi = 40$, according to Ref. 50. Open circles (crosses) indicate states to which quenches with nonconserved (or conserved, respectively) density have been made. Note that the identification of the structures near $\rho = 0.25$, 0.75 is controversial,[49-52] and hence quenches only in the region of the uncontroversial (2×1) structure are made.

$= [\psi^2(t)]^{1/2}$. By decomposing ψ into its contributions from individual unit cells $\psi_i(t)$ we obtain $\psi^2(t) = N^{-2}\sum_{ij}\psi_i(t) \cdot \psi_j(t)$. In the late stages of growth, the scalar product $\psi_i(t) \cdot \psi_j(t) \approx \psi_T^2$, ψ_T being the equilibrium value of the order parameter if i and j are sites within the same domain; if i and j are in different domains, the projection will average to zero. Hence we can estimate the order of magnitude of $\psi^2(t)$ as follows:

$$\psi^2(t) \approx N^{-2} N_d(t) L_d^4(t) \psi_T^2 \tag{16}$$

where the $\sum_{ij}$ was broken up in a sum over the $N_d(t)$ domains existing at time t, and the sum $\sum_{ij}\psi_i(t) \cdot \psi_j(t)$ where i, j are restricted to be in the same domain, of average linear dimension $Ld(t)$, yields $L_d^4(t)\psi_T^2$. Since any site must belong to a domain we conclude $N = N_d(t)L_d^2(t)$ and hence Eq. (16) reduces to

$$\psi^2(t) \equiv N^{-1} L_d^2(t) \psi_T^2 \tag{17}$$

This consideration suggests to *define* an effective domain linear dimension $L(t)$ as follows:

$$L(t) \equiv \sqrt{N}\left[\psi_1^2(t) + \psi_2^2(t)\right]^{1/2} / \psi_T \tag{18}$$

In an ordered monodomain sample, we have $L(t) = \sqrt{N}$, of course. We also note that the quantity $\psi^2(t)N^2$ would be experimentally simply accessible as the sum of the scattering intensities at the Bragg positions $\mathbf{Q}_1, \mathbf{Q}_2$ of the ordered structure,

$$\psi^2(t)N^2 = S(\mathbf{Q}_1, t) + S(\mathbf{Q}_2, t) \tag{19}$$

where $\mathbf{Q}_1 = \pi(1,0)$ and $\mathbf{Q}_2 = \pi(0,1)$ in our case.

Figure 6 shows then both the domain size $L(t)$ {Eq. (18)} and the excess energy $\Delta E(t) = E(t) - \langle E \rangle$. After a short transient period, both

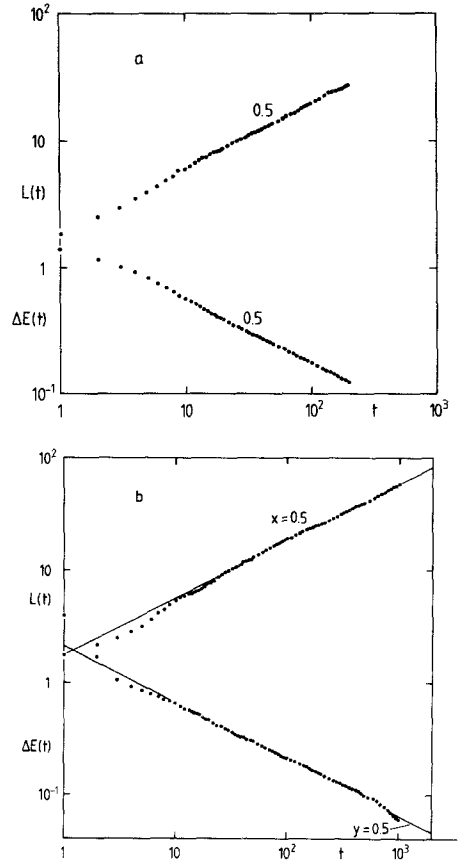

Fig. 6. Log–log plot of $\Delta E(t)$ and $L(t)$ vs. time, for the temperatures $T = 0.75$ (a) and $T = 1.33$ (b) Numbers at the curves are estimates of the exponents x and y, respectively. Temperature is measured in units of $|J_{nn}|$, and time in Monte Carlo steps per spin. Both cases represent averages over 45 samples of 80×80 lattices.

$L(t)$ and $\Delta E(t)$ follow nicely straight lines, i.e., they evolve in time according to the proposed power laws, Eq. (1), with

$$x = y = 1/2 \tag{20}$$

independent of temperature. The scaling relation $x = y$ has been generally proposed[33] on the grounds that in the late stages the excess energy in the system is due to the energy contained in the domain walls, and hence should be of order $|J_{nn}|N_d(t)L_d^{d-1}(t)/N$ in d dimensions. Invoking again $N_d(t)L_d^d(t) = N$, the relation $\Delta E(t) \propto L^{-1}(t)$ follows.

The exponent $x = 1/2$ agrees with results obtained for Ising models with nonconserved order parameter and $p = 2$[1,5,7,9,12,15] as well as with recent numerical simulations for a p-state Potts model[17] with $p \lesssim 6$. Our present results, as well as those of Ref. 17, indicate that the "locking-in mechanism" of domains[1,11] suggested to occur for $p > d + 1$, which would apply in our case, is not effective [as mentioned in the Introduction, this mechanism would imply $L(t) \propto \ln t$, i.e., $x = y = 0$].

We feel that the result $x = 1/2$ is not just due to a trivial extension of theories such as those[15,18] which deal with motion of random interfaces, because in our model there occur *several types of walls* (Fig. 7). While both

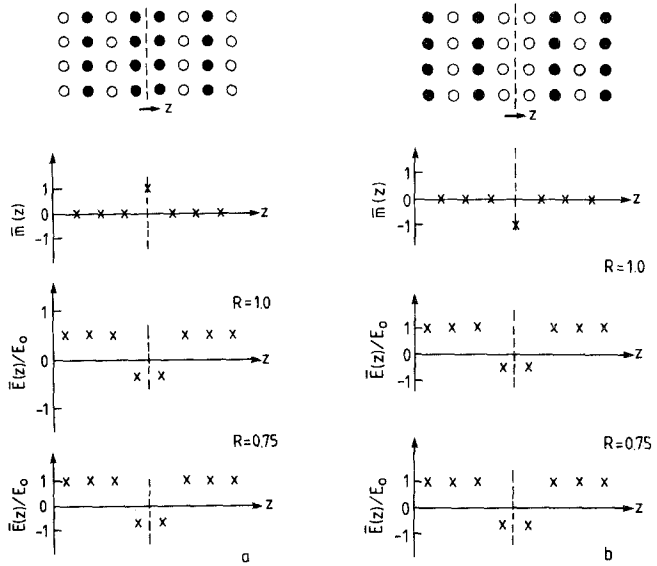

Fig. 7. Different types of walls between the ordered phases a, b, c, d of the (2×1) structure (cf. Fig. 1): (a) "superheavy" wall; (b) "superlight" wall; (c) "heavy" wall; (d) "light wall"; (e) "antiphase boundary"; (f) "45° wall." Underneath the arrangement of full and empty sites for each wall we display the profiles $\bar{m}(z)$ and $\bar{E}(z)$ of the magnetization and the energy, averaged along the wall, in the direction z perpendicular to the wall. All cases refer to $T = 0$.

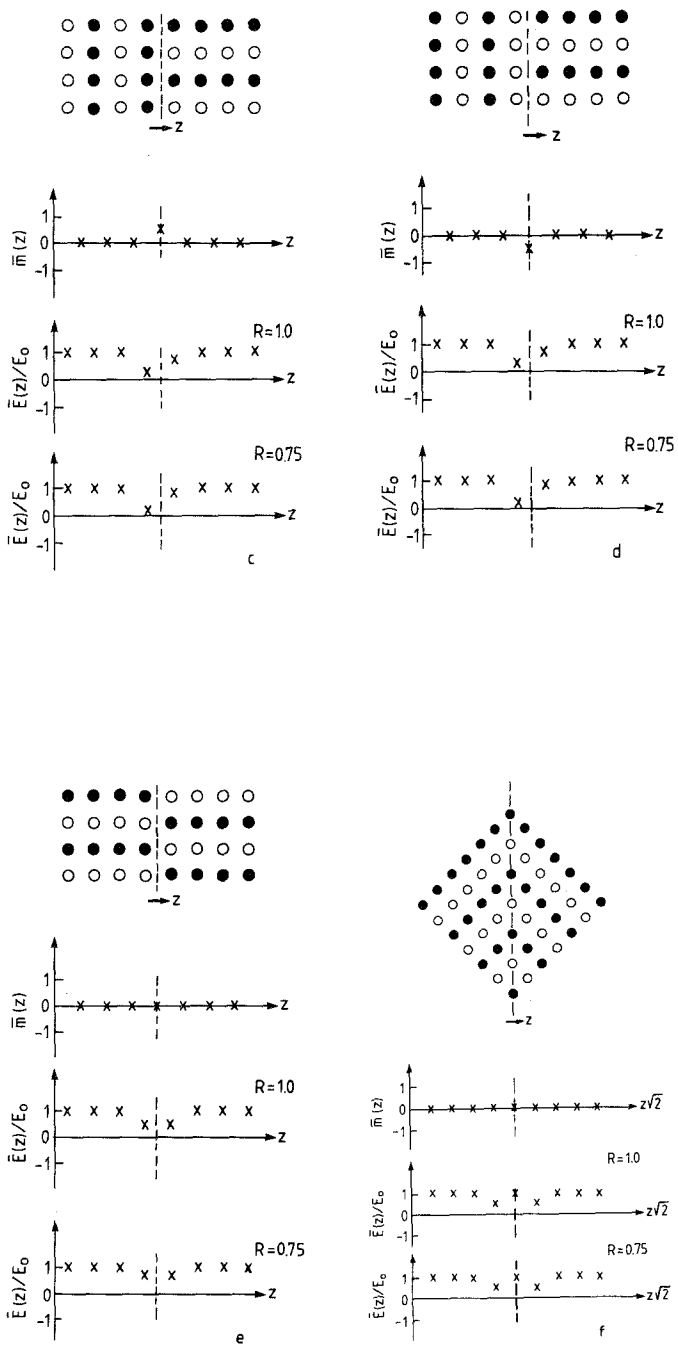

Fig. 7. Continued.

the "superheavy" and "superlight" wall are energetically very unfavorable, and hence such walls do no longer occur after a short transient period, the energy excess of the other types of walls is the same at $T = 0$. Thus one may have competition between different types of walls. Of course, one might expect that at finite temperature entropy considerations might lift the degeneracy between these walls, leading to a lower free energy of one (or some) wall(s) than the other ones. If this occurs, one would expect that the fraction of less favorable walls diminishes with increasing time after the quench.

In order to check whether this actually happens we have printed out many "snapshot pictures" of domain patterns, characterizing the various types of walls simply by their density excess (e.g., Fig. 8). At least at the

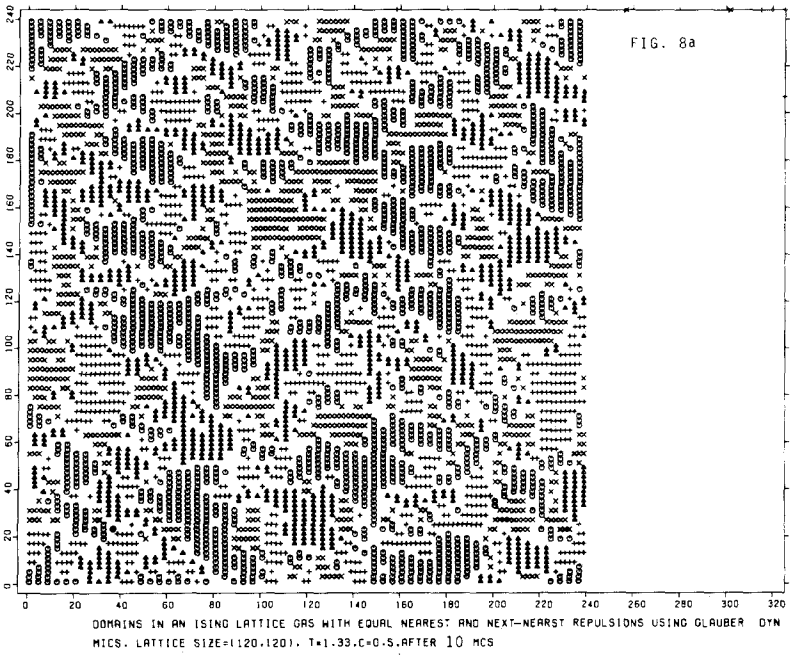

Fig. 8. A series of snapshot pictures of a time evolution of a 120×120 system at $T = 1.33$ and $H = 0$. Occupied sites are denoted by a circle if they belong to a domain of type a, by a triangle if they belong to domain of type b, by a lying cross if they belong to domain of type c, and by a standing cross if they belong to a domain of type d (cf. Fig. 1). Atoms belonging to walls are not shown. Times shown are $t = 10$ (a), 20 (c), 40 (e), 60 (g), 100 (i), 140 (k), 200 (m), 300 (o) and 400 (q). An alternative description in terms of the different walls at the corresponding times is shown in b, d, f, h, j, l, n, p, and r. There a 2×2 unit cell containing four atoms (superheavy wall) is denoted by a solid dot, a unit cell containing three atoms by a plus, a unit cell containing two atoms in diagonal configuration by an open circle, a unit cell containing one atom only by a vertical bar, and a cell with no atoms (superlight wall) by a star.

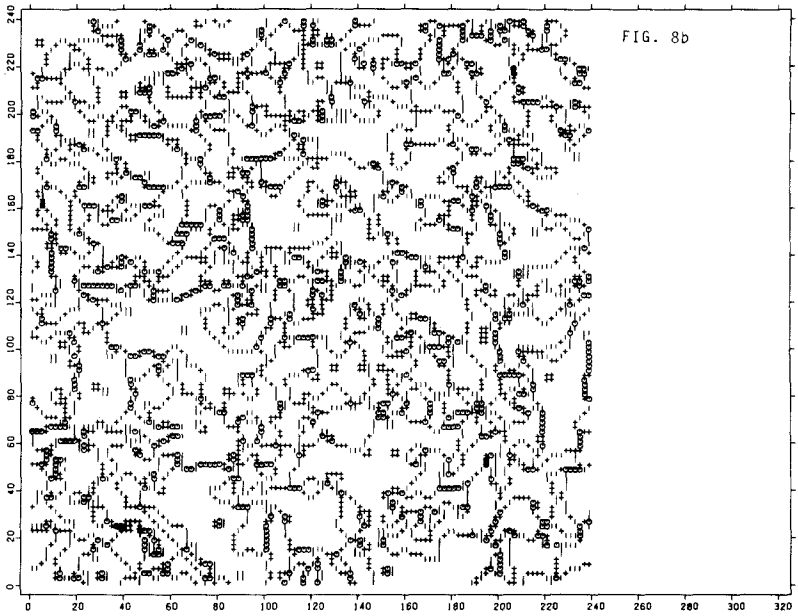

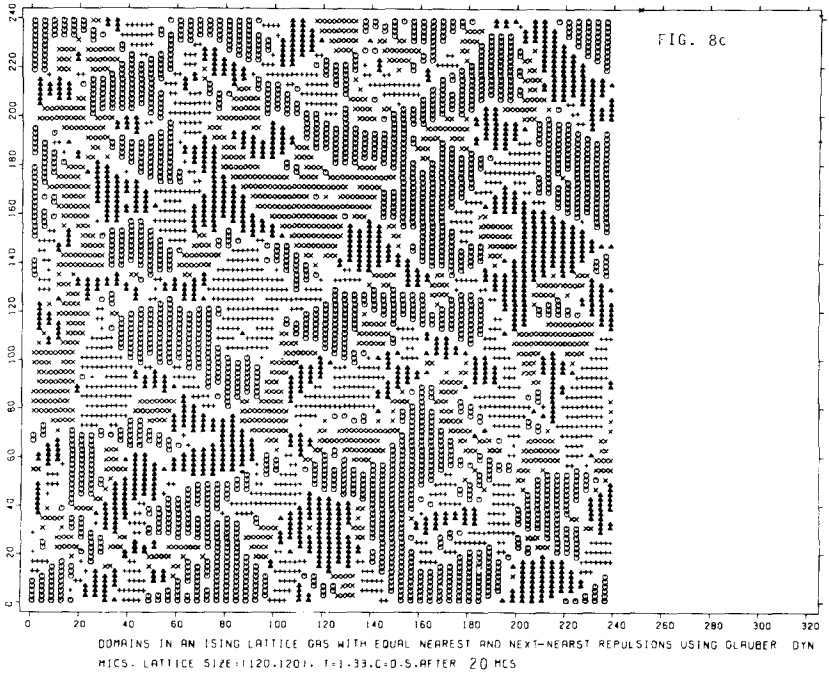

Fig. 8. Continued.

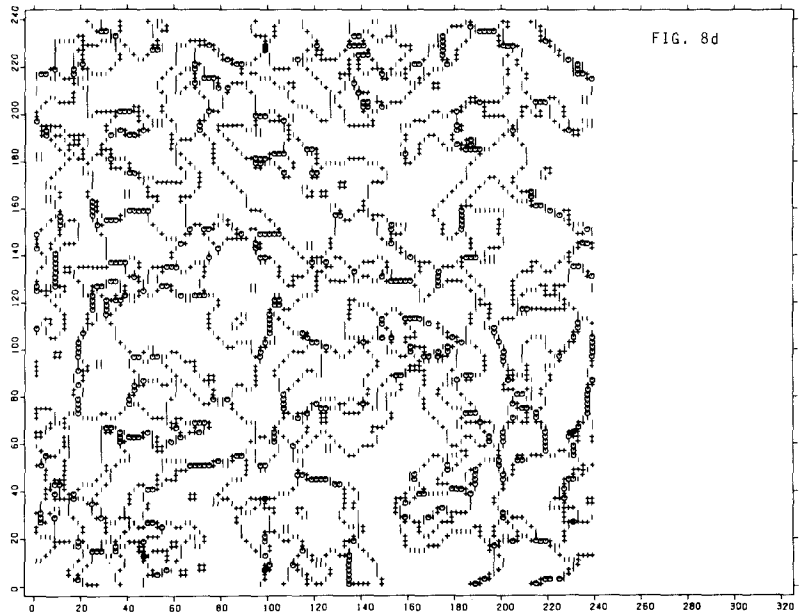

DOMAIN BOUNDRIES IN ISING LATTICE GAS WITH EQUAL NEAREST AND NEXT-NEARST REPULSIONS USING GLAUBER DYNMICS. LATTICE SIZE=(120,120). T=1.33,C=0.5,AFTER 20 MCS+ EXCESSMASS.- DEFICIT MASS.0 NO EXCESS MASS

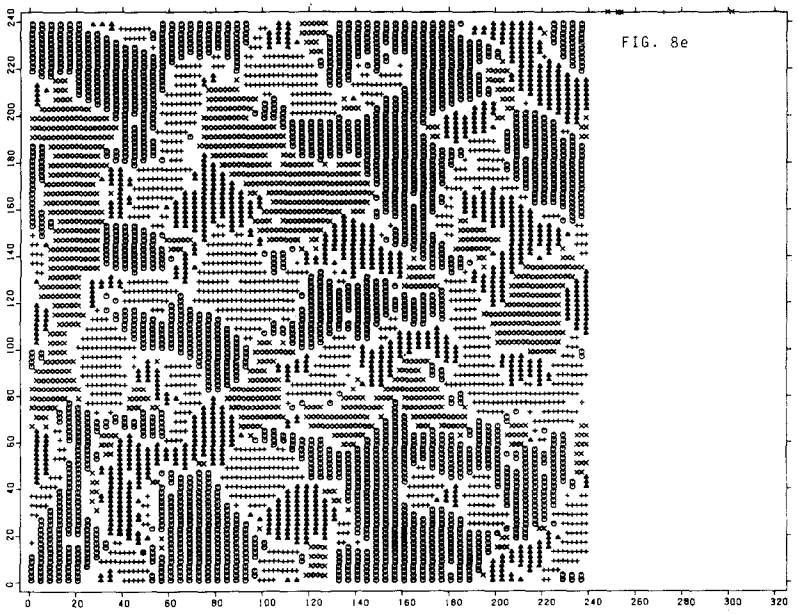

DOMAINS IN AN ISING LATTICE GAS WITH EQUAL NEAREST AND NEXT-NEARST REPULSIONS USING GLAUBER DYNMICS. LATTICE SIZE=(120,120). T=1.33,C=0.5,AFTER 40 MCS

Fig. 8. Continued.

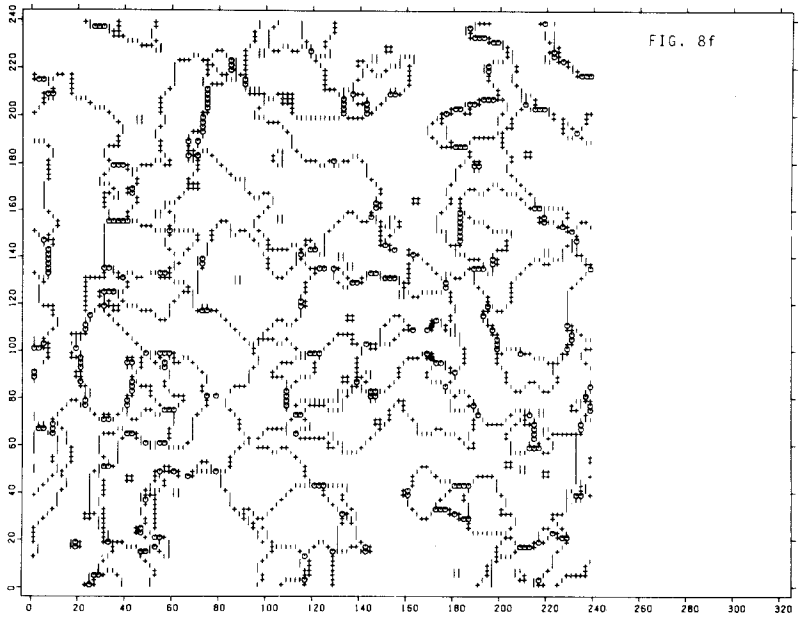

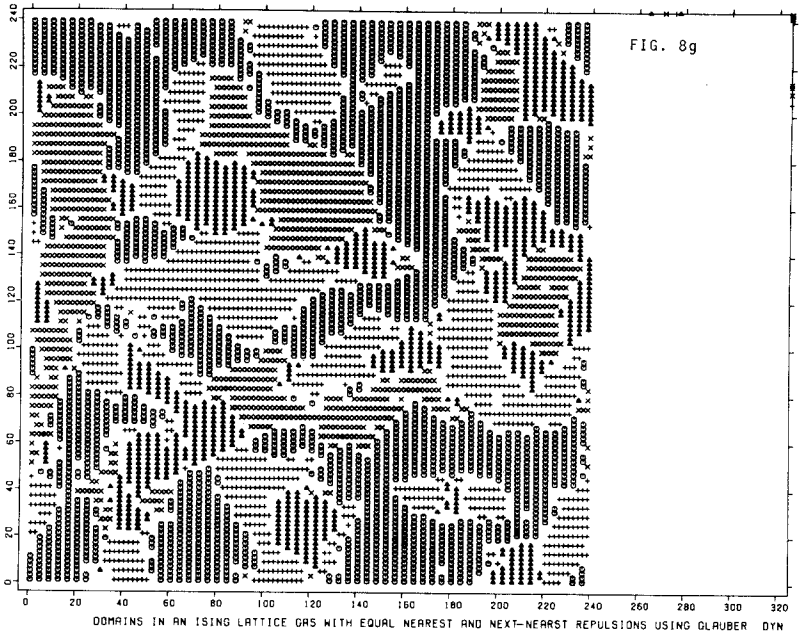

Fig. 8. Continued.

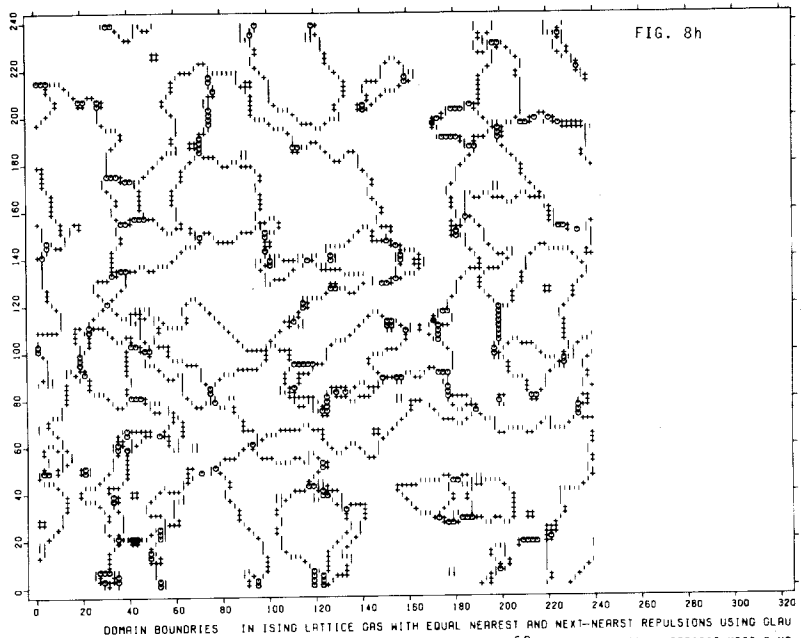

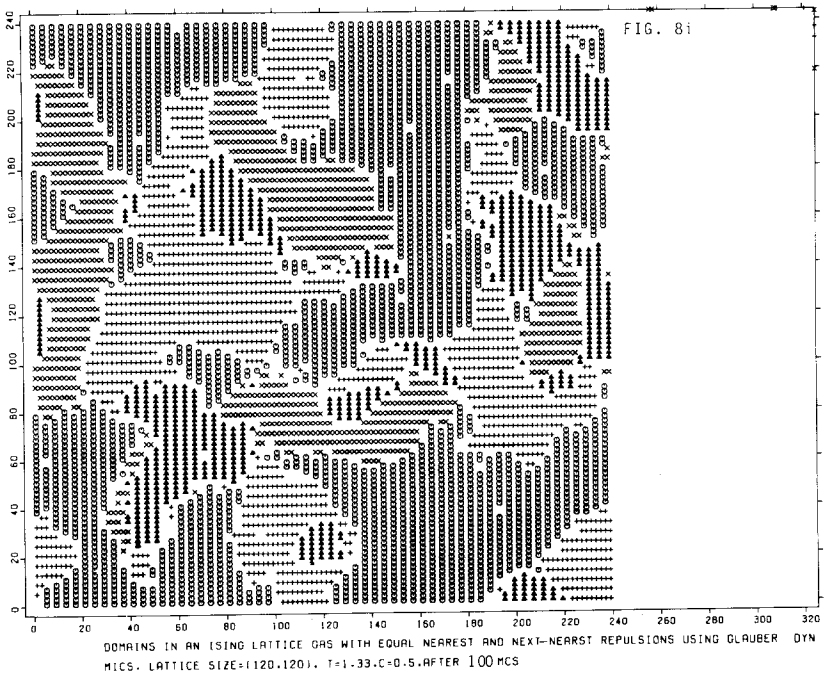

Fig. 8. Continued.

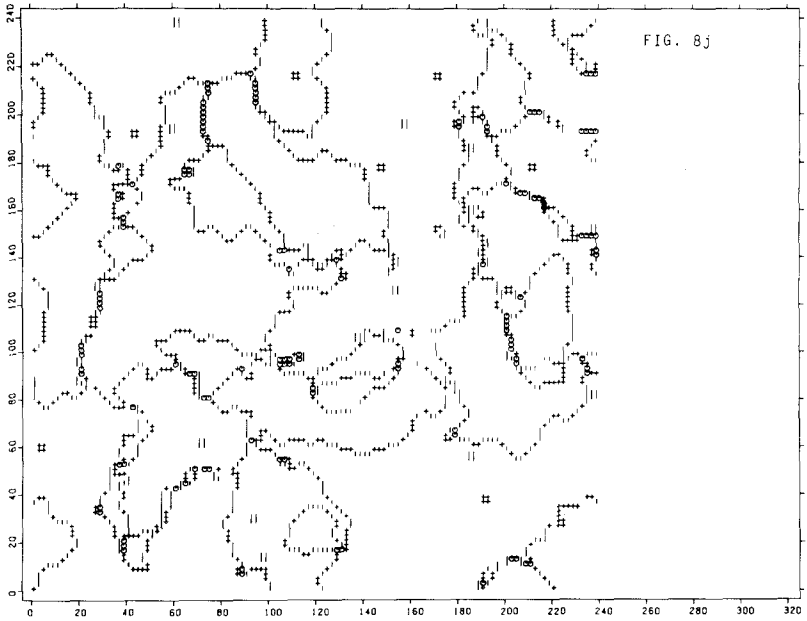

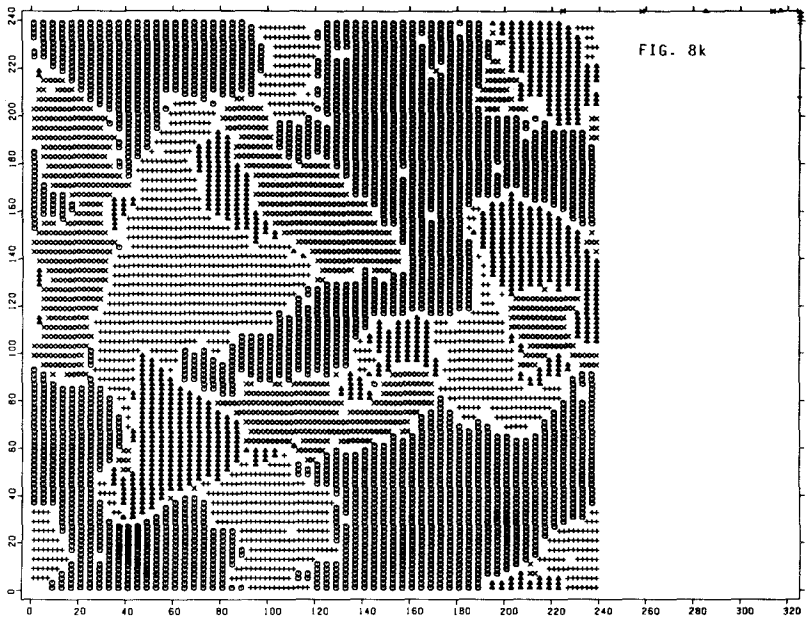

Fig. 8. Continued.

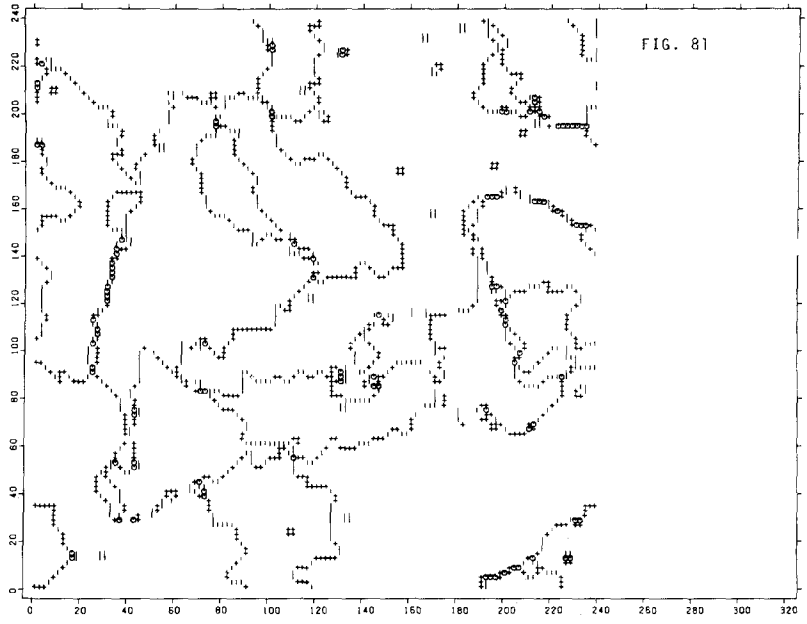

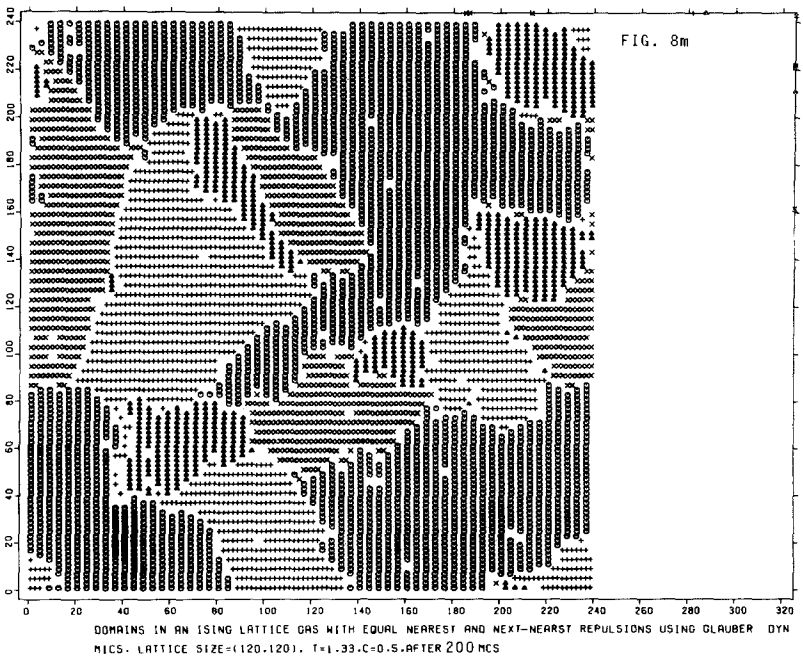

Fig. 8. Continued.

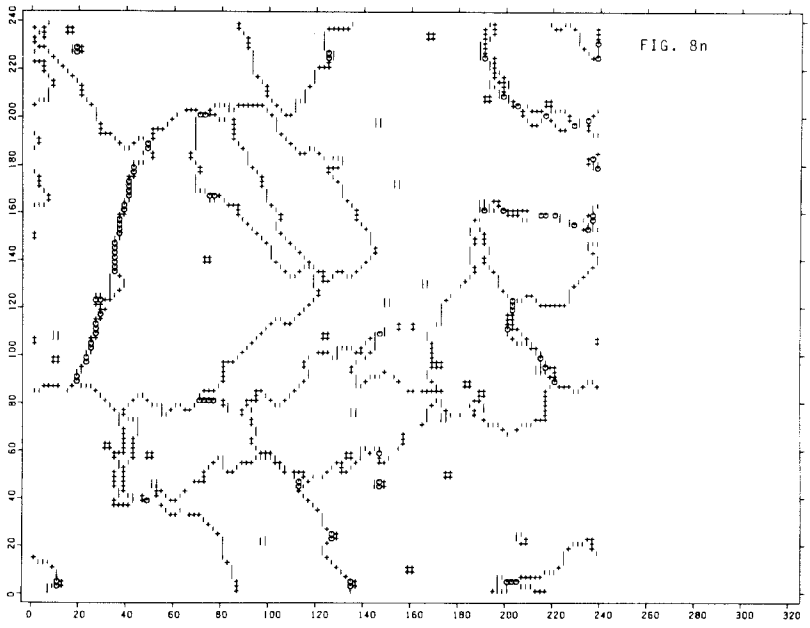

DOMAIN BOUNDRIES IN ISING LATTICE GAS WITH EQUAL NEAREST AND NEXT-NEARST REPULSIONS USING GLAUBER DYNMICS. LATTICE SIZE=(120,120). T=1.33,C=0.5,AFTER 200MCS. EXCESSMASS.- DEFICIT MASS,0 NO EXCESS MASS

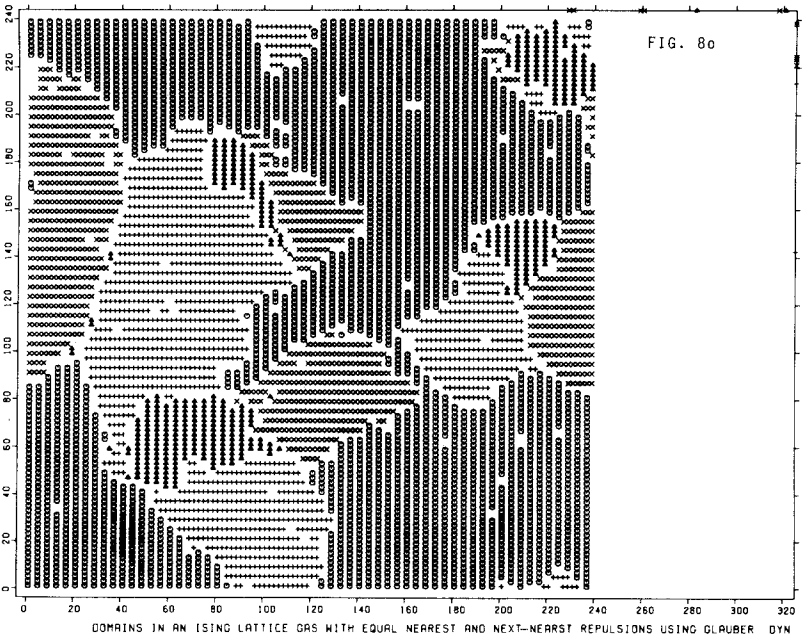

DOMAINS IN AN ISING LATTICE GAS WITH EQUAL NEAREST AND NEXT-NEARST REPULSIONS USING GLAUBER DYNMICS. LATTICE SIZE=(120,120). T=1.33,C=0.5,AFTER 300 MCS

Fig. 8. Continued.

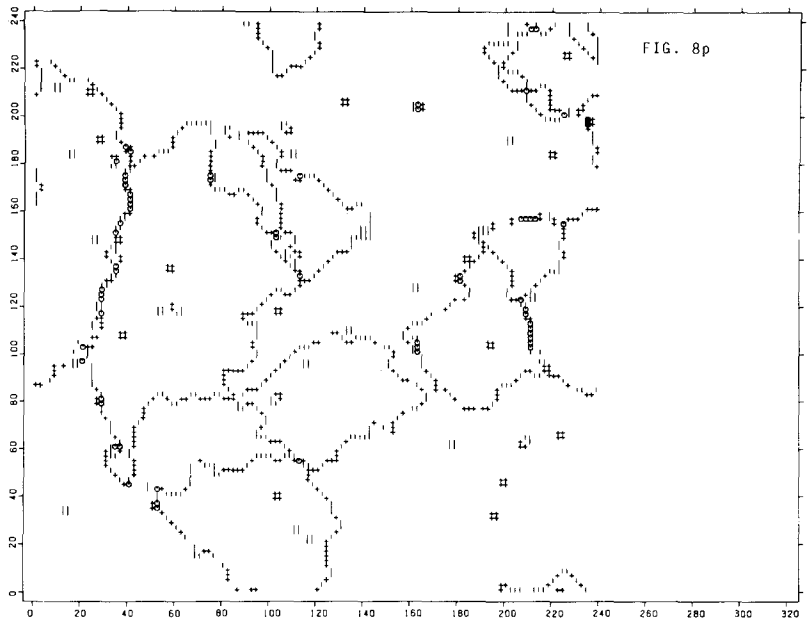

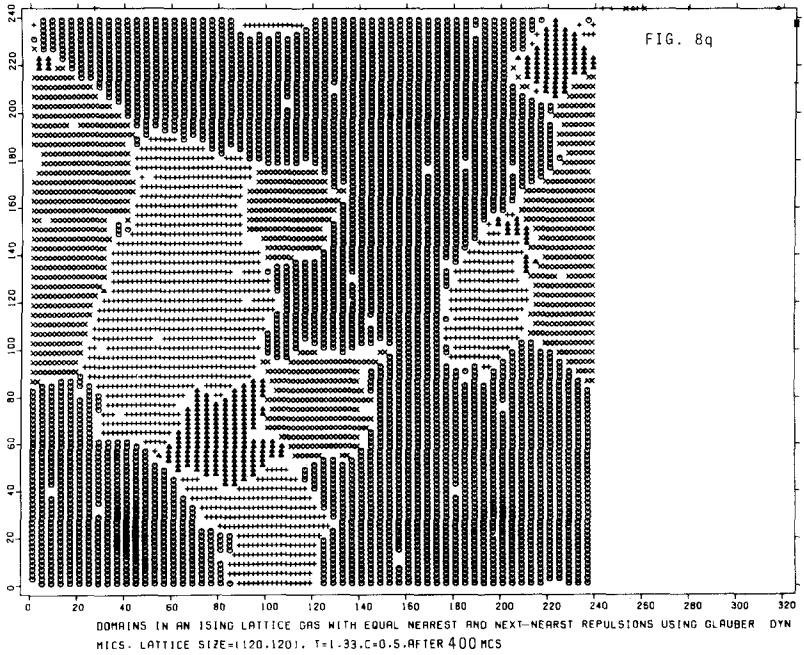

Fig. 8. Continued.

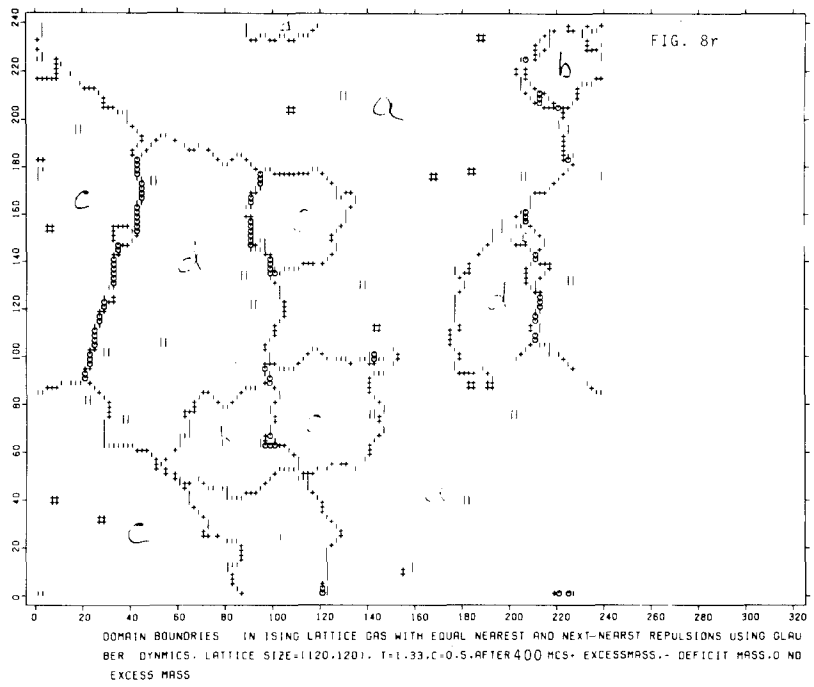

Fig. 8. Continued.

considered temperatures, all types of walls seem to survive with about equal probability. This means that either the walls remain degenerate in free energy up to the critical point, or their free energy differences are so small that one would have to watch the domain pattern over a significantly longer period of time than we were able to do to see this effect. Of course, for $\phi_{nn} \neq \phi_{nnn}$ a simple "bond-counting" analysis shows that already at $T = 0$ the degeneracy is lifted.

Next we turn to the behavior of the structure factor. We have obtained both $S(\mathbf{Q}_1 + \mathbf{k}, t)$ and $S(\mathbf{Q}_2 + \mathbf{k}, t)$, choosing the direction of $\mathbf{k}$ perpendicular to $\mathbf{Q}_1$ or $\mathbf{Q}_2$, respectively, since then the calculation of the structure factor simplifies and the program runs much faster than for general direction of $\mathbf{k}$. Then we add both terms together and thus obtain the analog of Eq. (19) for finite k. By this procedure we greatly reduce the statistical fluctuations. The resulting structure factor $S(q, t)$ (Fig. 9) is qualitatively similar to structure factors obtained for Ising models with $p = 2$.[8–10] Figure 10 demonstrates that for $T = 0.75$ and 1.33 it indeed nicely satisfies the scaling hypothesis, Eq. (2). Thus the halfwidth $\sigma(t)$ of the structure

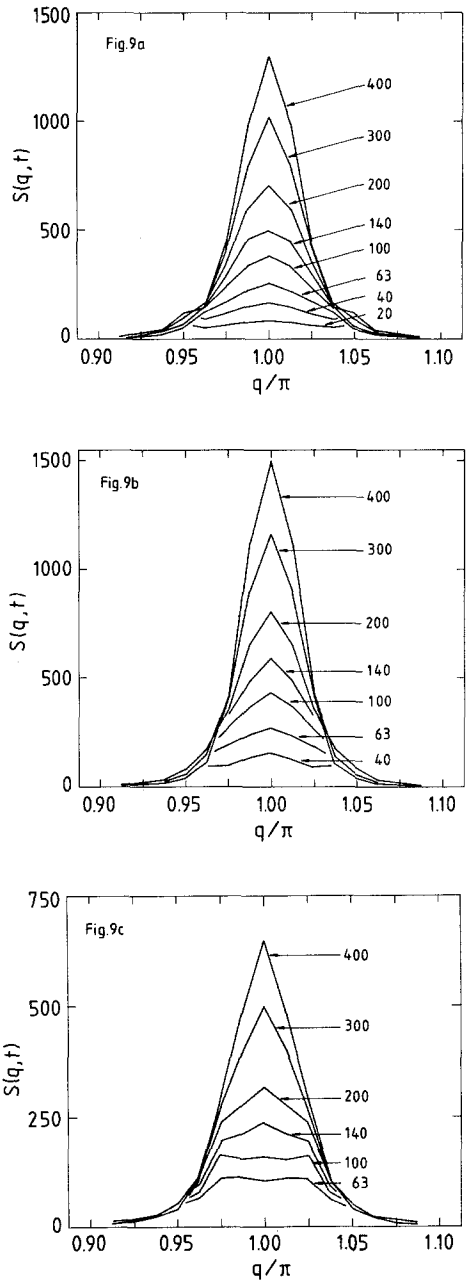

Fig. 9. Structure factor $S(q, t)$ plotted vs. q at $H = 0$ and $T = 1.33$ (a), 0.75 (b), and 2.0 (c). Parameter of the curves is the time t, measured in Monte Carlo steps per spin. Data were obtained from averages over 250 runs, using a lattice of size 160×160. Note that because of the finite size and periodic boundary conditions $S(q, t)$ is defined for the discrete set of points $\mathbf{q}$ only [see Eq. (9)]. For simplicity we have connected $S(q, t)$ at these discrete values by straight lines. Note that $S(q, t)$ at each time t actually is an average $\int_{-\Delta t}^{\Delta t} S(q, t + t')\, dt'/(2\Delta t)$, with $\Delta t/t \approx 0.1$.

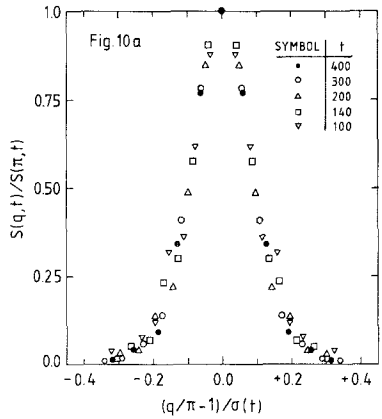

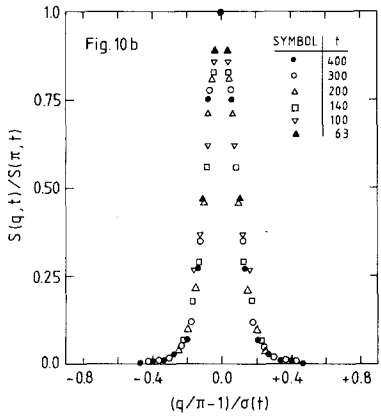

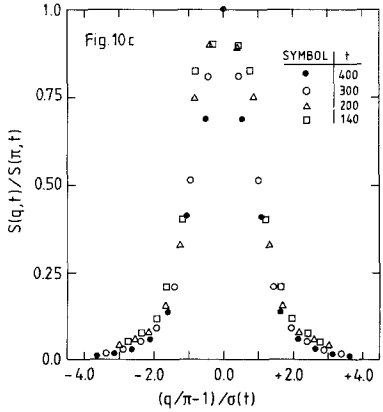

Fig. 10. Structure factor plotted in scaled form, normalizing $S(q, t)$ by its peak value $S(\pi, t)$ and normalizing $q/\pi - 1$ by the halfwidth $\sigma(t)$, for $T = 1.33$ (a), $T = 0.75$ (b), and 2.0 (c). Figure 10b resembles a simple Gaussian. There are, however, systematic deviations from the Gaussian form in the wings of the distribution.

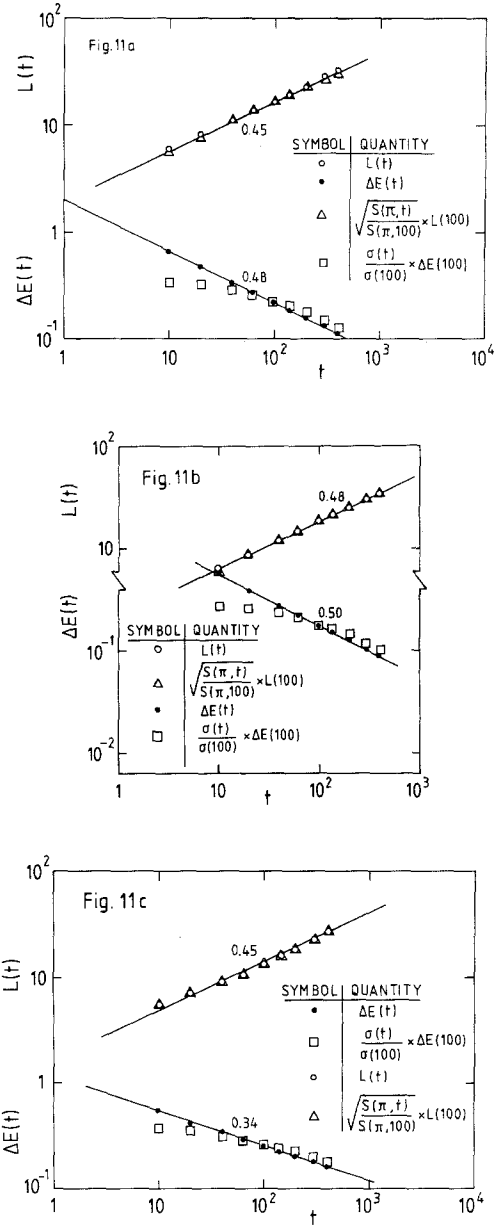

Fig. 11. Log–log plot of domain size $L(t)$, energy excess $\Delta E(t)$, peak height $S(\pi, t)$ of this structure factor and its halfwidth $\sigma(t)$ plotted vs. time, for $T = 1.33$ (a), $T = 0.75$ (b), and 2.0 (c). Here $\sigma(t)$ and $[S(\pi, t)]^{1/2}$ are normalized such that they coincide with $\Delta E(t)$ and $L(t)$ at $t = 100$.

factor also satisfies a power law, Fig. 11:

$$\sigma(t) \propto t^{-x_\sigma}, \qquad \text{with} \quad x_\sigma = x = 1/2 \tag{21}$$

It would be interesting to calculate the scaling functions both for the case $p = 2$ and the present case with high precision, in order to be able to check whether they also are identical. For $T = 2.0$, on the other hand, we observe more pronounced deviations from scaling (Fig. 10c), and the various exponents seem to no longer agree with each other (Fig. 11c). We interpret these observations as crossover toward critical relaxation (Section 6).

As a remark on the accuracy of our numerical procedures, we note that $[S(\pi, t)]^{1/2}$, which has been smoothed by integrating over time intervals Δt (Fig. 9), agrees very well with the data for $L(t)$ obtained directly in independent calculations from Eq. (18) where $\psi_1^2(t), \psi_2^2(t)$ were recorded at much shorter time intervals and also the smoothing interval could be chosen much smaller (i.e., of the order of the distance between two successive points in Fig. 6 at each time).

4. ORDERING KINETICS WITH "KAWASAKI DYNAMICS"

In this section we consider quenches to the same temperatures in the ordered region as in the previous section, but treat now the case of conserved density. Again we start with a discussion of the time evolution of the domain size $L(t)$ and energy excess $\Delta E(t)$, Fig. 12. While for $T = 1.33$ after a short transient period both $L(t)$ and $\Delta E(t)$ evolve according to the power laws Eq. (1), over several decades in time, with

$$x = y \approx 0.35 \tag{22}$$

the power-law description for $T = 0.75$ is not so good: over an intermediate interval of domain sizes $4 \lesssim L(t) \lesssim 10$, a power-law behavior is observed but with distinctly smaller exponents, $x = y \approx 0.20$. The curvature seen particularly in $\Delta E(t)$ at late times may indicate that there a crossover sets in to the exponents quoted in Eq. (22). Since we find (Section 5) that in quenches to $T = 0$ with conserved density the system gets trapped in a metastable domain state, i.e., curves for $L(t), \Delta E(t)$ bend over to a finite value $L(\infty)$ and a nonzero value $\Delta E(\infty)$ at late times, i.e., $x = y = 0$ at $T = 0$, we feel that the data at $T = 0.75$ are affected by crossover effects, i.e., the system nearly gets trapped over intermediate time scales.

Of course, arguing that the simulation data for $T = 0.75$ may reflect crossover one must ask oneself whether the data for $T = 1.33$ may be affected by crossover as well. It is difficult to rule this out with certainty:

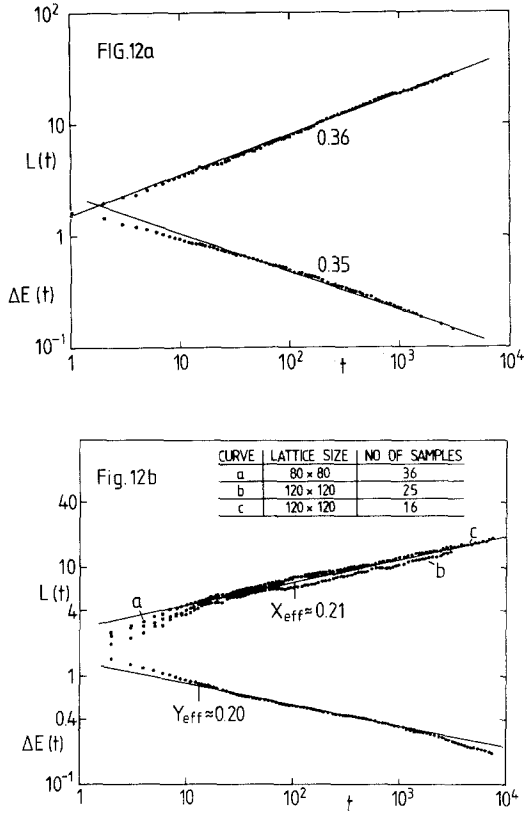

Fig. 12. Log–log plot of $\Delta E(t)$ and $L(t)$ vs. time, for the case of conserved density $\rho = 1/2$, at temperatures $T = 1.33$ (a) and 0.75 (b). In case (a) the points are averages of 32 samples of a 120×120 system; in case (b) the lattice sizes and number of samples is indicated in the figure. Numbers at the curves indicate the estimates for the resulting exponents x, y.

taking data closer to the phase boundary at $T = 1.33$ by varying ρ (Fig. 13) one starts to see effects of crossover toward critical relaxation (see Section 6): effective exponents x_{eff}, y_{eff} are no longer equal, while x_{eff} stays around the value given by Eq. (22), y_{eff} seems to increase significantly. As we shall show in Section 6, the scaling law $x = y$ is no longer valid for critical relaxation. Similarly, when we stay at $\rho = 1/2$ but increase T to 1.61, the exponent x_{eff} increases to about 0.4, while y stays at about 0.35. Although such a systematic variation of exponents with parameters such as density or temperature could be a real effect, as suggested by Furukawa,[48] our data are certainly also consistent with the interpretation that in the limit $t \to \infty$ the exponents x, y are universal inside the whole ordered region $0 < T$

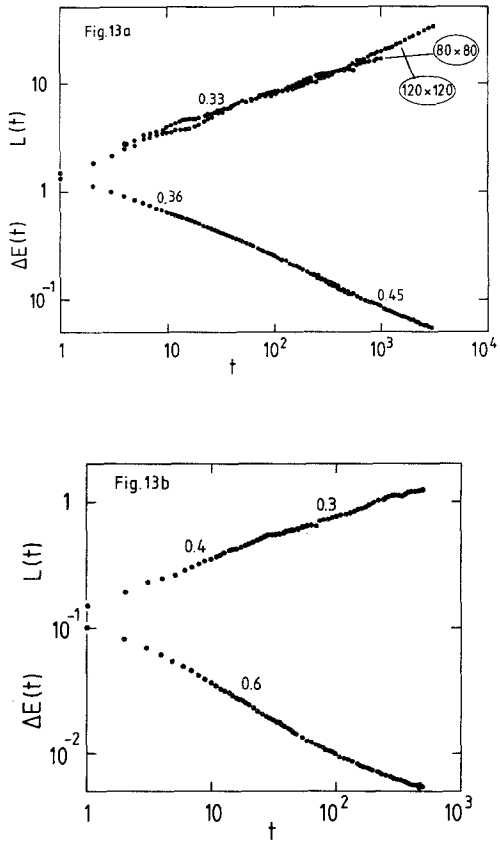

Fig. 13. Log–log plot of $\Delta E(t)$ and $L(t)$ vs. time, for the temperature $T = 1.33$ and the case of conserved density, at $\rho = 0.456$ (a) and 0.398 (b). Lattice sizes are indicated in the figure. Data points are averages over 25 runs.

$< T_c(\rho)$, but near $T = 0$ and near $T_c(\rho)$ one observes crossover to other mechanisms controlling the asymptotic relaxation at $T = 0$ and $T = T_c(\rho)$, respectively. The correct values of the asymptotic exponents are then most reliably estimated in a region of the phase diagram where one stays away from the crossover regimes as far as possible. Since the point $T = 1.33$, $\rho = 1/2$ fulfils this criterion, the time evolution at this point shows no evidence for crossover, and the exponents x, y estimated for other points in the phase diagram around this point (Fig. 5) are similar, we suggest that Eq. (22), within error limits of about ± 0.05, should be the true asymptotic exponent. This conclusion is corroborated by Fig. 14, where the exponent $y_{\text{eff}}(t)$, fitted to various time intervals, is plotted vs. temperature for ρ

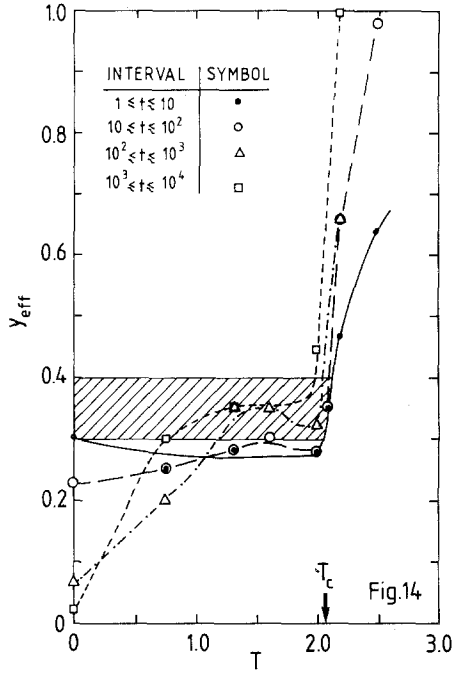

Fig. 14. Effective exponent y_{eff} obtained from fitting $\Delta E(t) \propto t^{-y_{\text{eff}}}$ over one decade in time, for various time intervals as shown in the figure, plotted vs. temperature. Curves are only guides to the eye. The asymptotic exponent y is estimated to be within the shaded region.

$= 1/2$. The proposed asymptotic behavior for $y_{\text{eff}}(t \to \infty) \equiv y$ is

$$\begin{aligned} y = 0, \quad T = 0; \qquad y = 0.35 \pm 0.05, \quad 0 < T < T_c; \\ y = y_c, \quad T = T_c; \qquad y = 1, \quad T > T_c \end{aligned} \tag{23}$$

Since in the previous section we have seen that the result $y = 1$ for $T > T_c$ is easily missed because of finite-size effects, it is absolutely essential, of course, to make sure that the estimates given in Eqs. (22), (23) are no artefacts of finite size as well. Thus we have studied the time evolution at $T = 1.33$, $\rho = 0.5$ varying the lattice size from 80×80 to 800×800, Fig. 15. It is seen that the resulting estimates are scattered in the interval $0.3 \lesssim x$, $y \lesssim 0.4$, but we are not able to detect any systematic decrease of y with increasing size, as it happened for $T > T_c$. The absence of finite-size effects which would be due to the lack of small k in terms relaxing with factors $e^{-D_{\text{eff}}k^2 t}$ is plausible, of course, since at the chosen temperature the collective diffusion constant D in thermal equilibrium is extremely small,[58] and hence the "bulk" contribution to the energy relaxation is negligible in

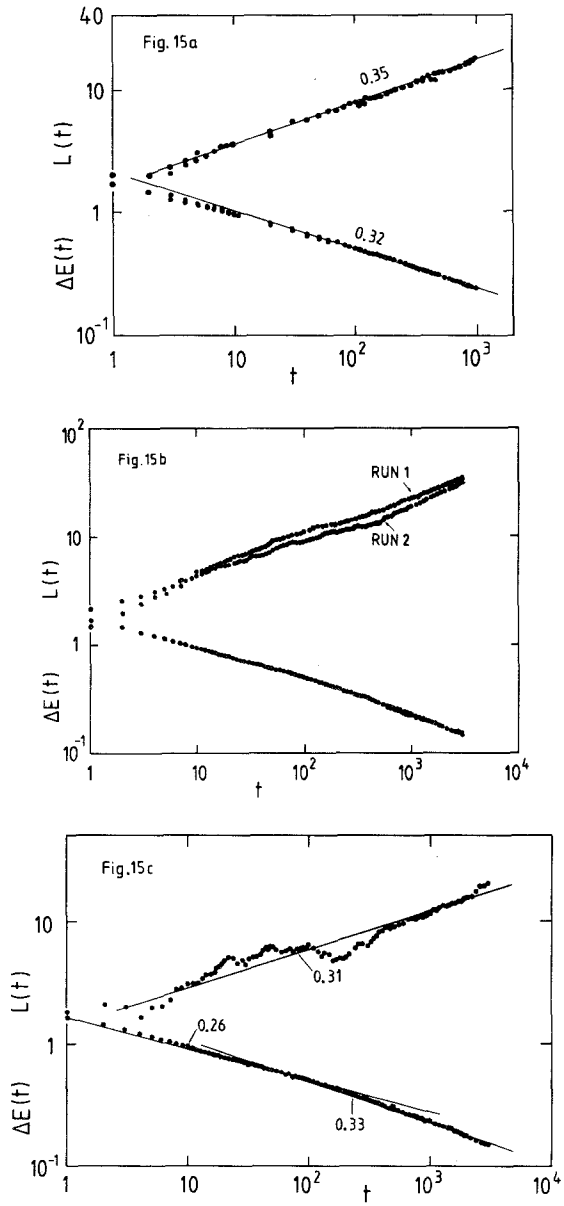

Fig. 15. Log–log plot of $\Delta E(t)$ and $L(t)$ vs. time, for the temperature $T = 1.33$ and $\rho = 1/2$, and the lattice sizes 80×80 (a), 200×200 (b), 400×400 (c), and averaged over all sizes (d). In case (a), two averages of 100 samples each are shown: in case (b), two averages of four samples; in case (c) one average of four samples; all these data and a run of 800×800 lattice (e) are averaged together with the data of Fig. 12a to yield Fig. 15d.

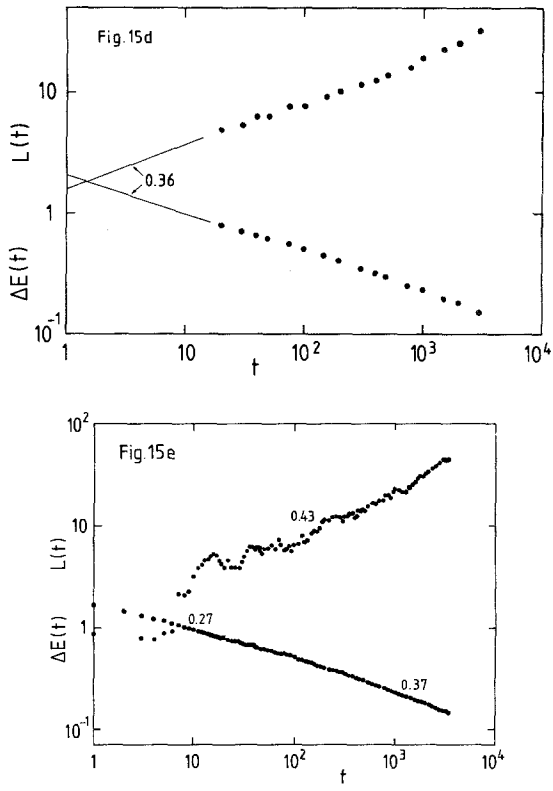

Fig. 15. Continued.

comparison with the contribution due to walls. For $t \lesssim 10^2$, there is a consistently smaller effective exponent in the energy relaxation. We interpret this as the onset of crossover effects to the locking-in of domain states at $T = 0$, where over intermediate regime of times (seen more clearly at $T = 0.75$) exponents intermediate between $y = 0$ and $y = 0.35$ are seen. Note that for $\sqrt{N} \geqslant 200$ the average domain size reached at the time where the simulation was stopped is still about an order of magnitude smaller than $\sqrt{N}$, or even less. Thus the other finite size effects discussed in Section 2 are not expected to be of importance here either.

What is remarkable in Fig. 15 is the slow approach to the thermodynamic limit of $L(t)$, as far as statistical fluctuations are concerned. This behavior is in marked contrast to the behavior of $\Delta E(t)$: fluctuations of $\Delta E(t)$ are reduced with increasing size N in the expected way. This observation calls for a statistical theory for fluctuations of domain growth.

The structure factor $S(q, t)$ was obtained as described in Section 3 and is shown in Fig. 16; again evidence for the scaling law Eq. (2) is obtained

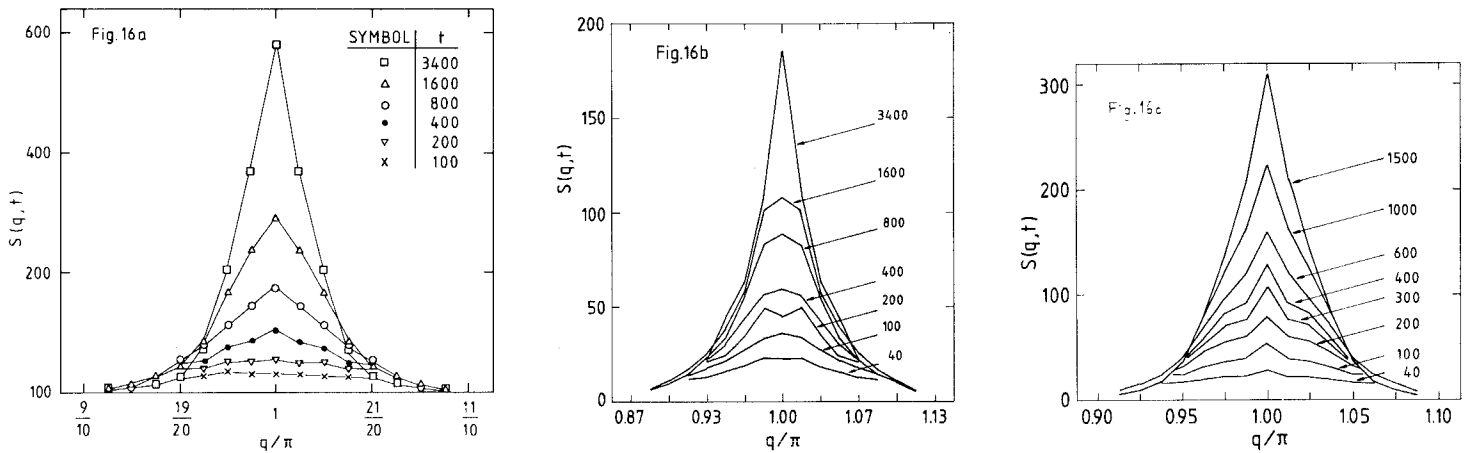

Fig. 16. Structure factor $S(q,t)$ plotted vs. q at different times (measured in Monte Carlo steps per particle) for $T = 1.33$ (a) and $T = 0.75$ (b), for the case of conserved density $\rho = 1/2$ and $T = 1.33$, $\rho = 0.453$ (c). Data for $T = 1.33$ are computed from 135 (a) or 250 (b) runs of a system of size 160×160, while data for $T = 0.75$ are from a system of size 120×120, averaging 235 runs (for times $\leqslant 400$) and 135 runs at larger times.

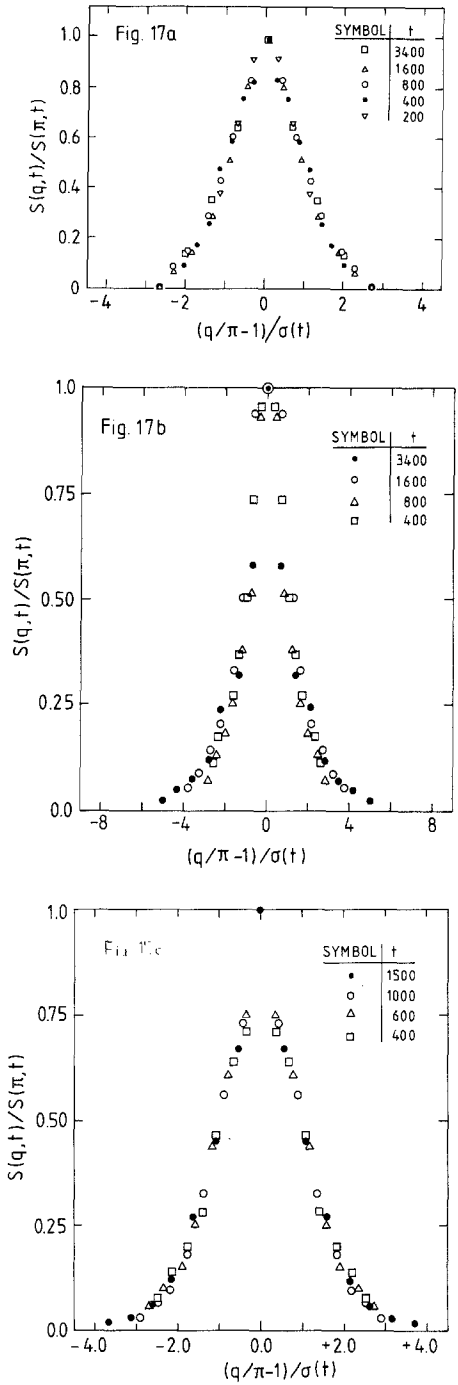

Fig. 17. Structure factor for the case of conserved density plotted in scaled form, normalizing $S(q,t)$ by its peak value $S(\pi,t)$ and normalizing $a/\pi - 1$ by the halfwidth $\sigma(t)$, for $\rho = 1/2$, $T = 1.33$ (a) and $T = 0.75$ (b), and for $\rho = 0.453$, $t = 1.33$ (c).

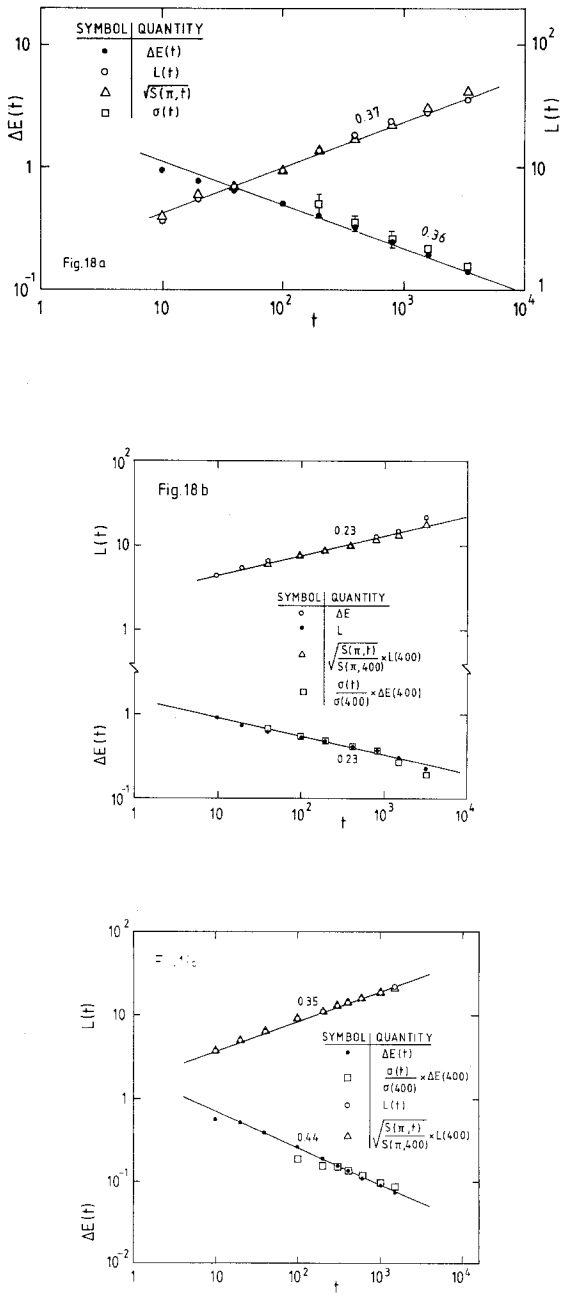

Fig. 18. Log–log plot of domain size $L(t)$ energy excess $\Delta E(t)$, peak height $S(\pi, t)$ of the structure factor and its halfwidth $\sigma(t)$ plotted vs. time, for $T = 1.33$ $\rho = 1/2$ (a), and $T = 0.75$ (b), and for $T = 1.33$, $\rho = 0.452$ (c). Here $[S[\pi, t)]^{1/2}$ and $\sigma(t)$ are normalized such that they coincide with $L(t)$ and $\Delta E(t)$, respectively, at $T = 100$ (a) or $t = 400$ (b).

(Fig. 17). It appears that the scaling behavior is not strictly valid when the time variation of $L(t)$ is not yet in the asymptotic regime, as can be seen from the systematic discrepancies in the wings of the distribution (Fig. 17b). This observation is further evidence that the exponents $x \approx y \approx 0.23$ as obtained in Fig. 18b are not yet characteristic for the asymptotic behavior but rather due to crossover effects, as discussed above.

Figure 19 then shows typical snapshot pictures of the domain patterns and the type of walls prevailing during domain growth with conserved density. As in the nonconserved case, domain shapes are rather irregular throughout growth, and four types of walls ("heavy," "light," "antiphase," "45 degree") seem to persist throughout the late stages.

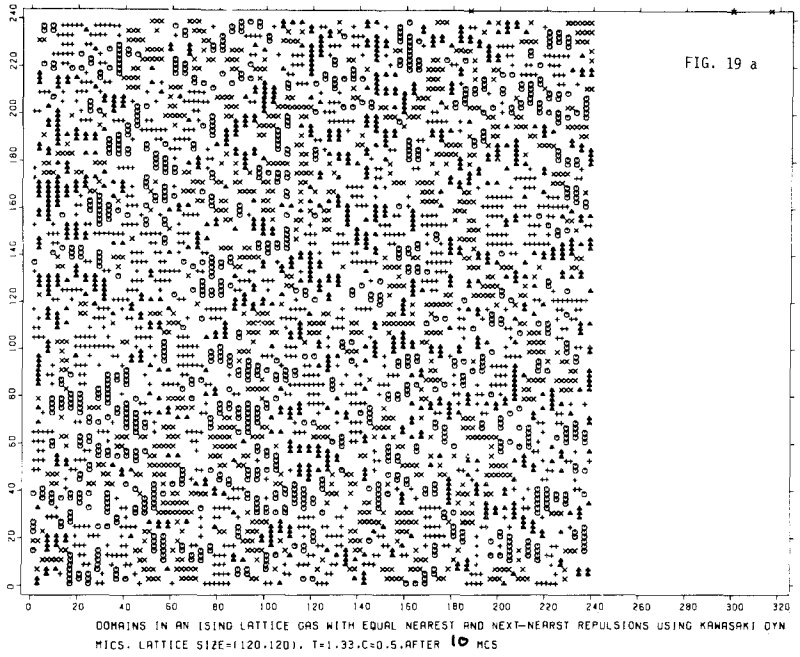

Fig. 19. A series of snapshot pictures of a time evolution of a 120×120 system at $T = 1.33$ and $\rho = 0.45$ at conserved density. Occupied sites are denoted by a circle if they belong to a domain of type a, by a triangle for domain b, by a lying cross if they belong to a domain of type c, and by a standing cross if they belong to a domain of type d (cf. Fig. 1). Atoms belonging to walls are not shown. Times shown are $t = 10$ (a), 20 (c), 40 (e), 65 (g), 100 (i), 140 (k), 200 (m), 300 (o), 500 (q), 800 (s), 1200 (u), 1700 (w), an alternative description in terms of the different walls at the corresponding times is shown in (b)–(x). There a 2×2 unit cell containing four atoms (superheavy wall) is denoted by a solid dot, a unit cell containing three atoms by a plus, a unit cell containing two atoms in diagonal configuration by an open circle, a unit cell containing one atom only by a vertical bar, and a cell with no atoms (superlight wall) by a star.

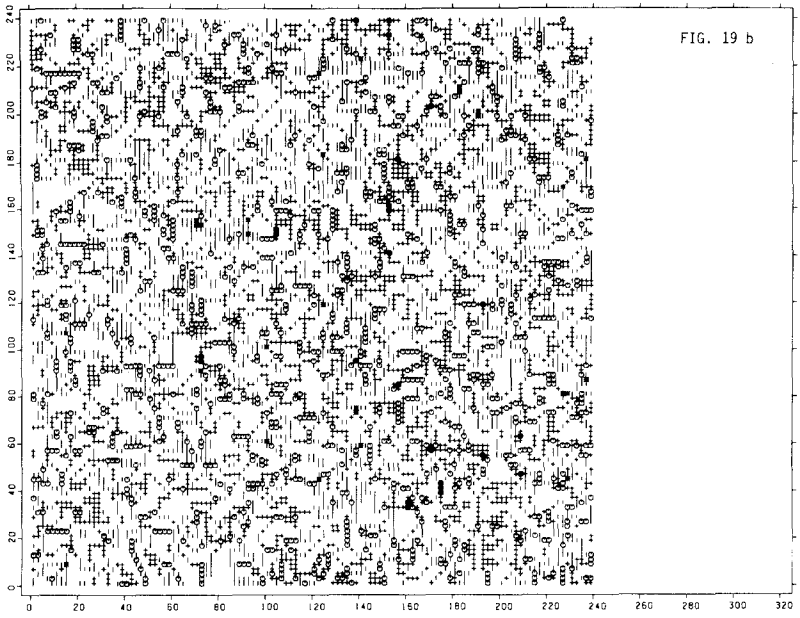

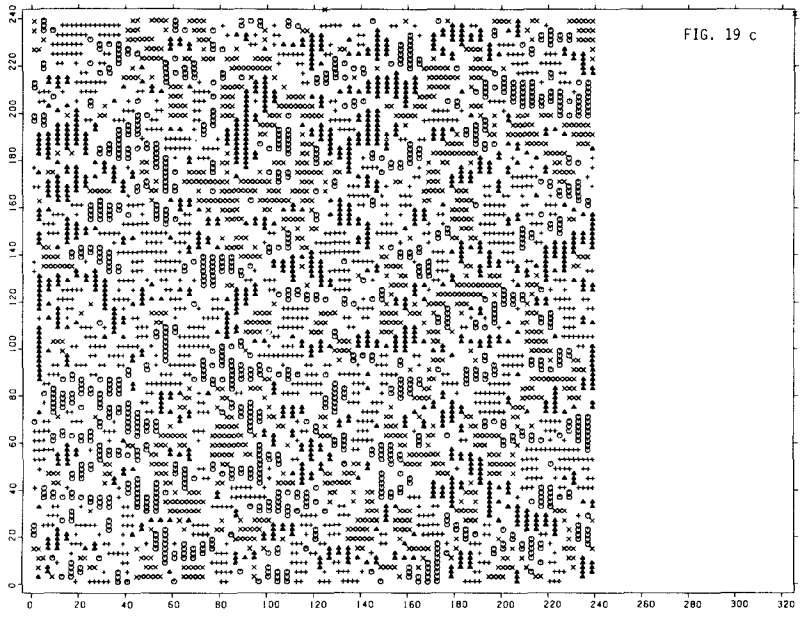

Fig. 19. Continued.

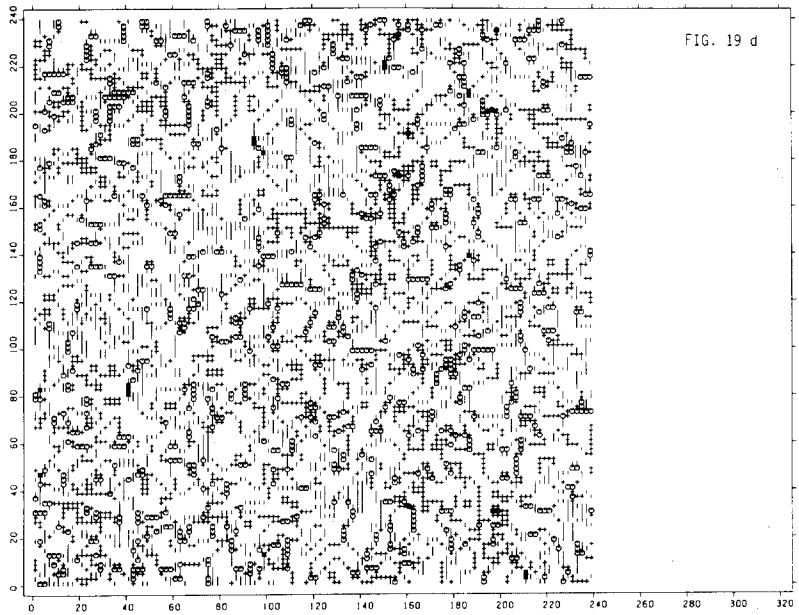

DOMAIN BOUNDRIES IN ISING LATTICE GAS WITH EQUAL NEAREST AND NEXT-NEARST REPULSIONS USING KAWASAKI DYNMICS. LATTICE SIZE=(120,120), T=1.33,C=0.5,AFTER 20 MCS. EXCESSMASS.- DEFICIT MASS.O NO EXCESS MASS

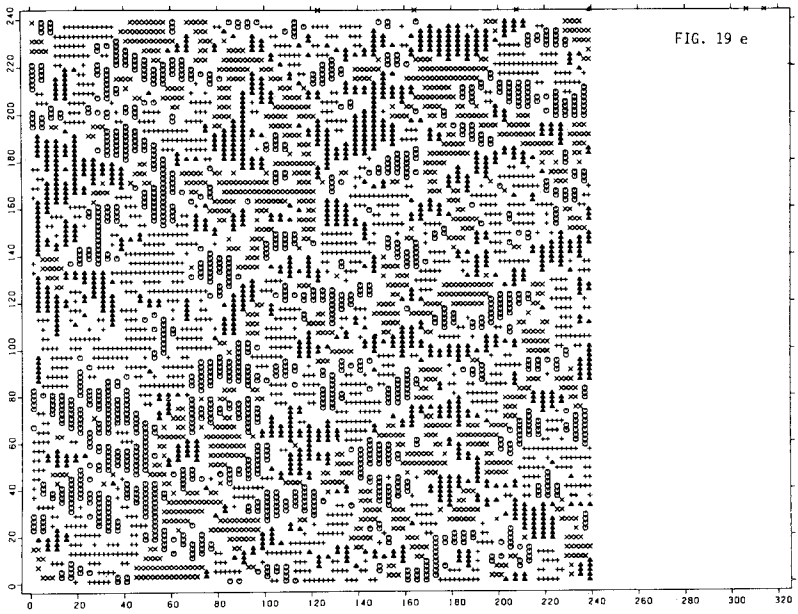

DOMAINS IN AN ISING LATTICE GAS WITH EQUAL NEAREST AND NEXT-NEARST REPULSIONS USING KAWASAKI DYNMICS. LATTICE SIZE=(120,120), T=1.33,C=0.5,AFTER 40 MCS

Fig. 19. Continued.

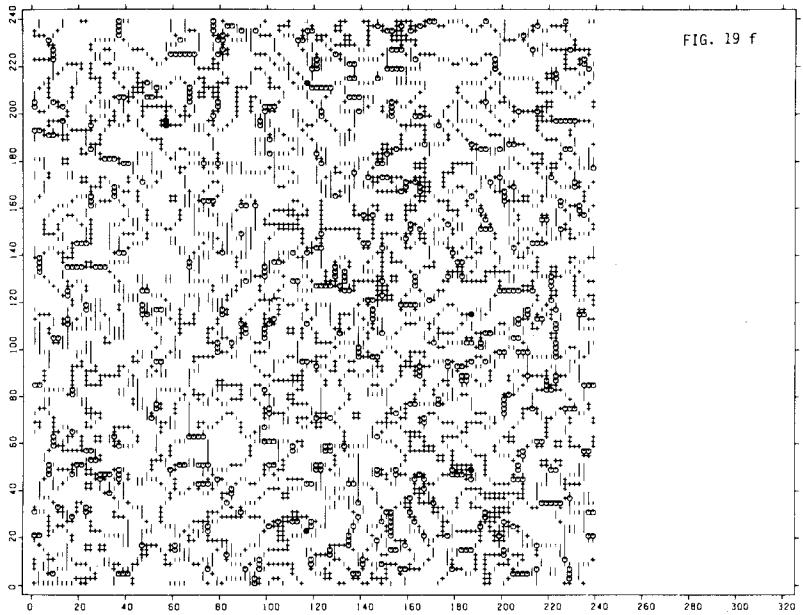

Fig. 19. Continued.

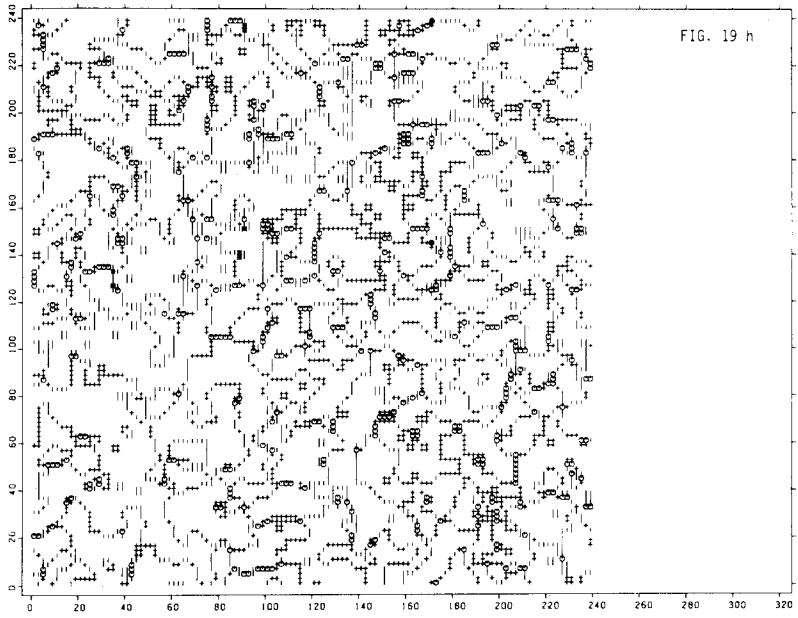

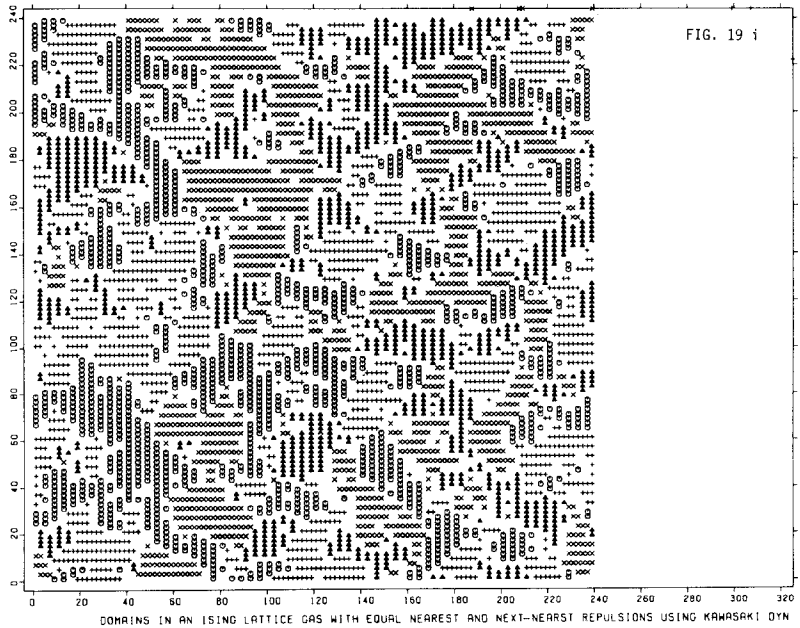

Fig. 19. Continued.

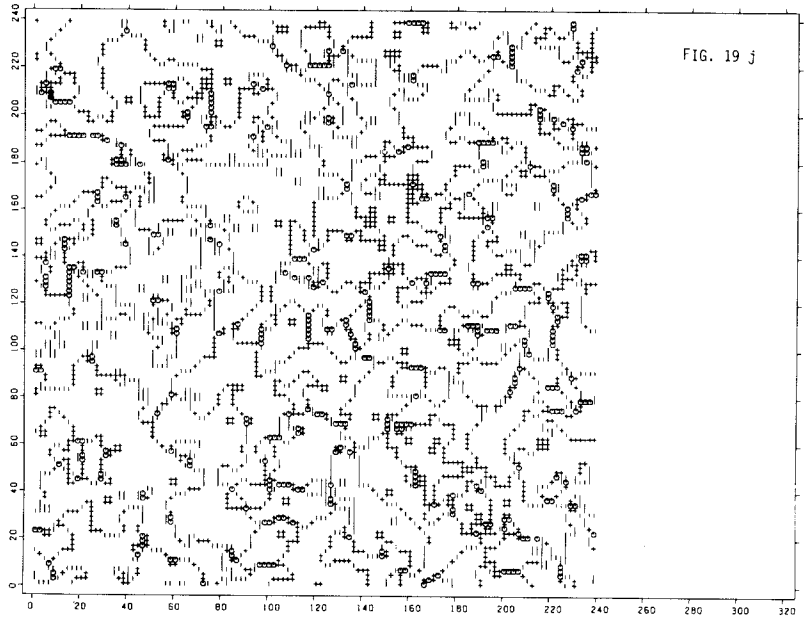

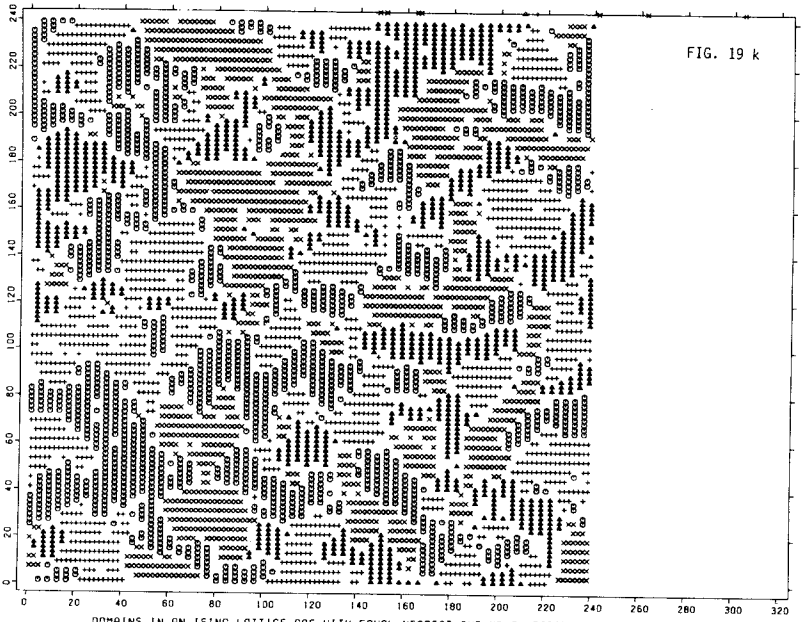

Fig. 19. Continued.

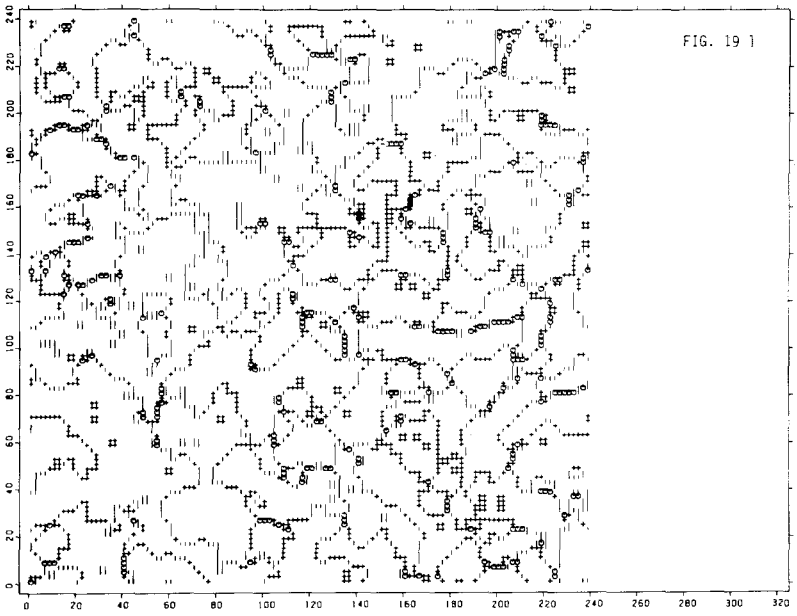

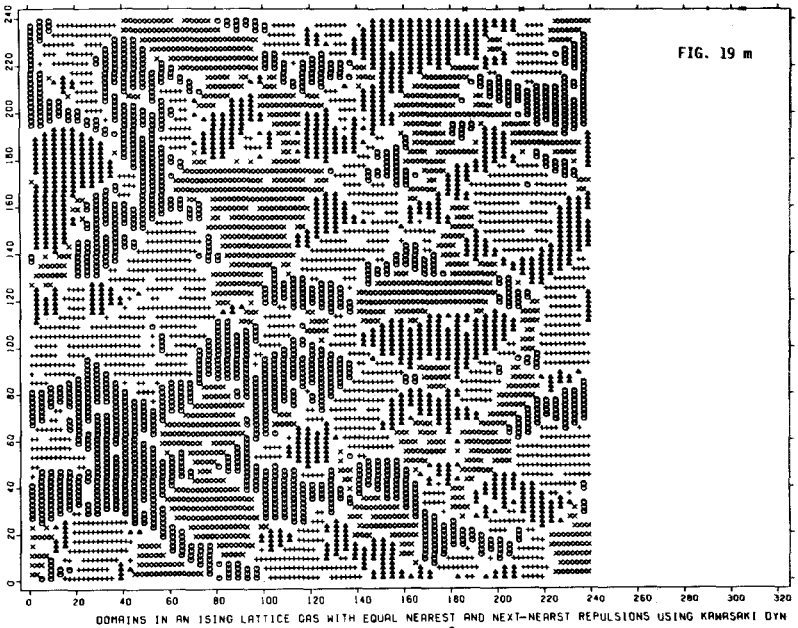

Fig. 19. Continued.

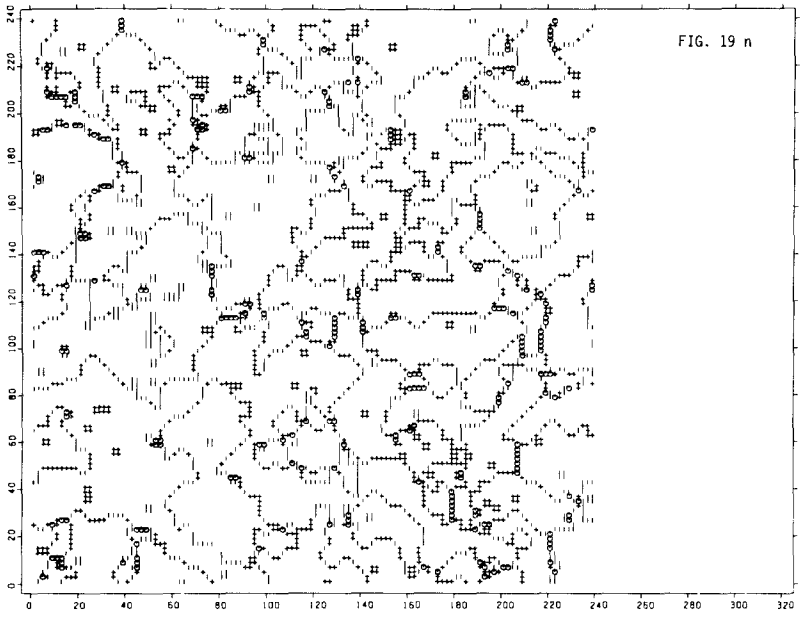

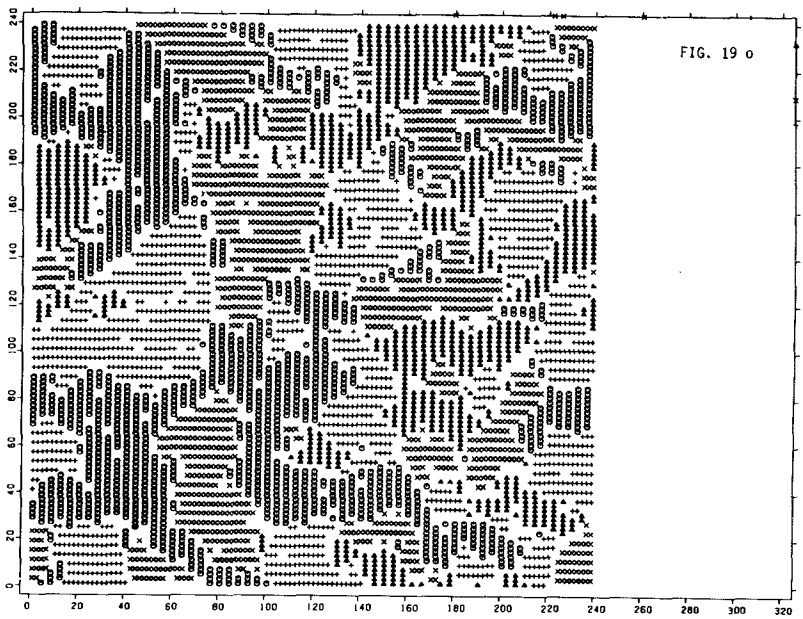

Fig. 19. Continued.

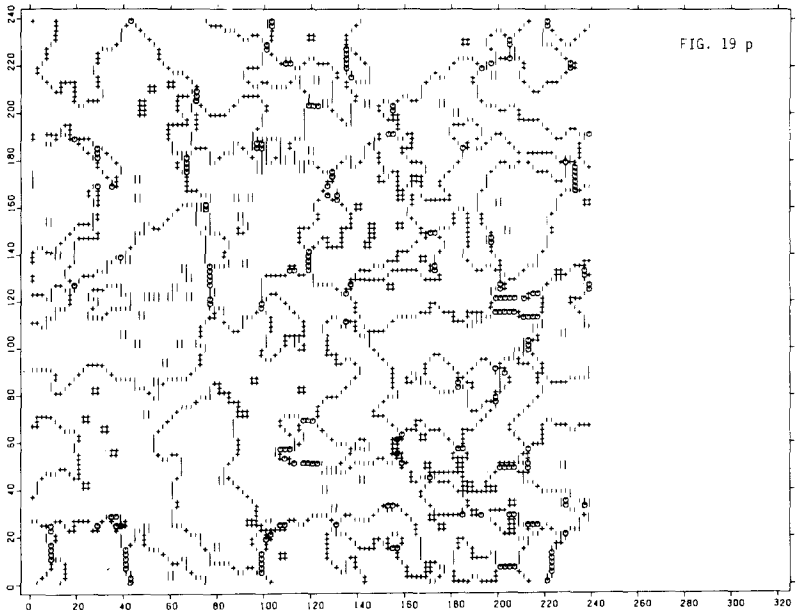

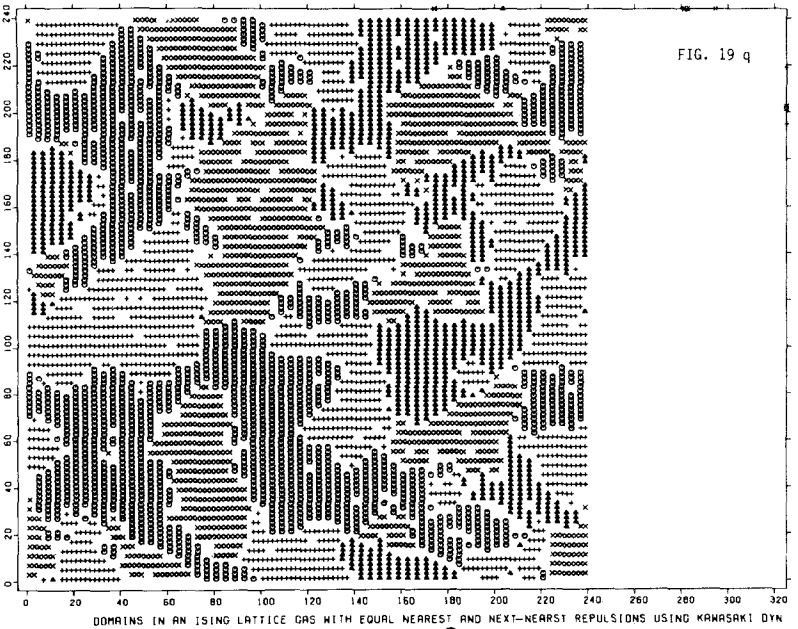

Fig. 19. Continued.

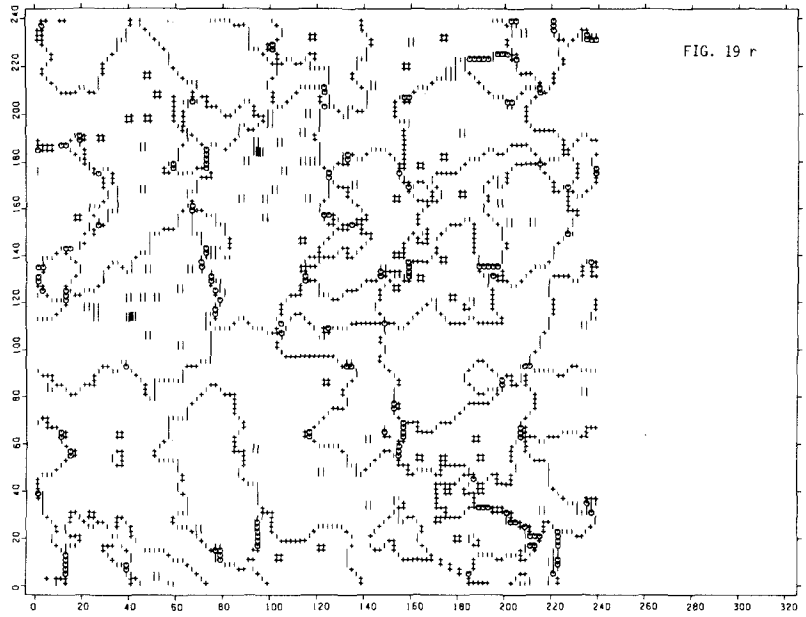

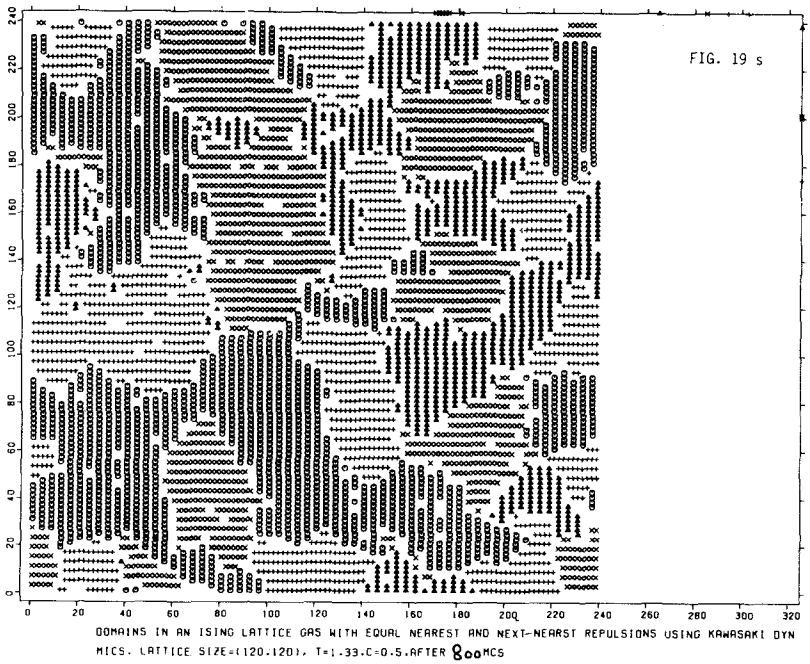

Fig. 19. Continued.

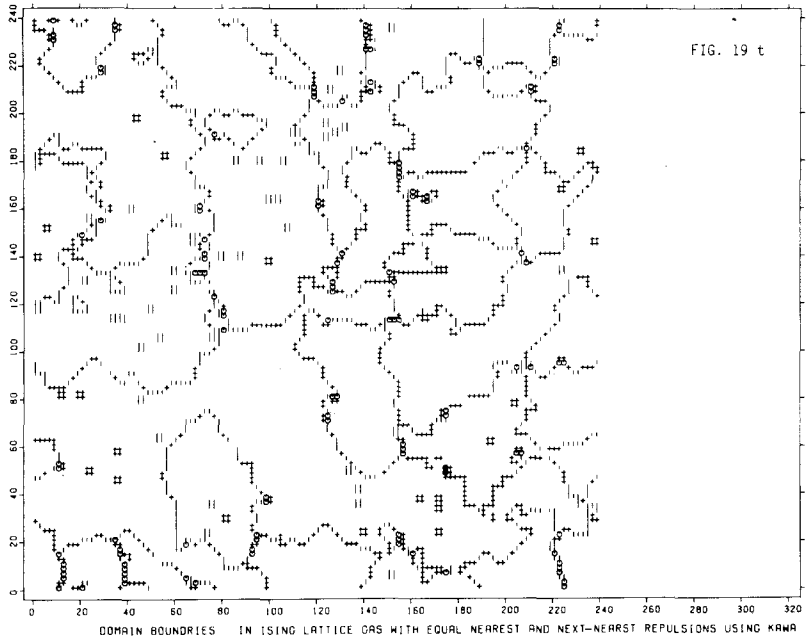

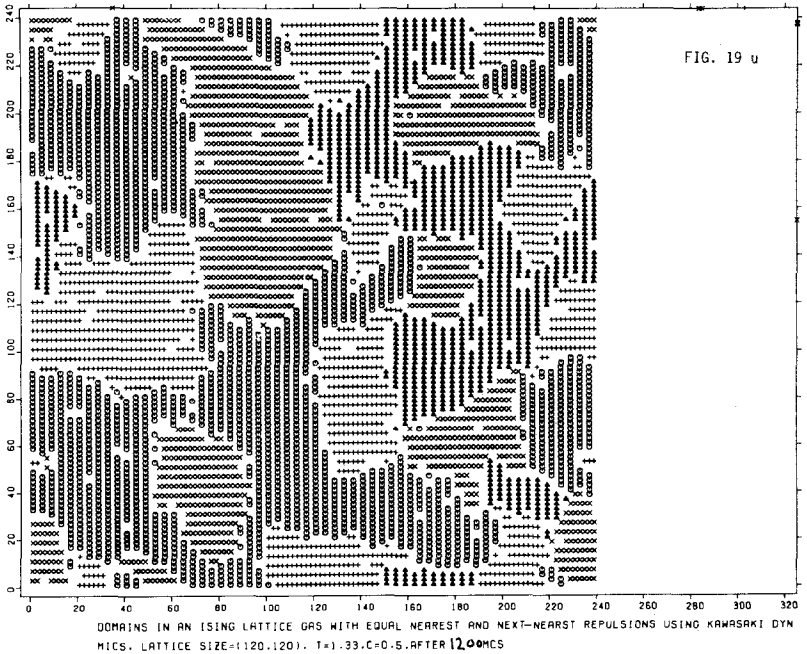

Fig. 19. Continued.

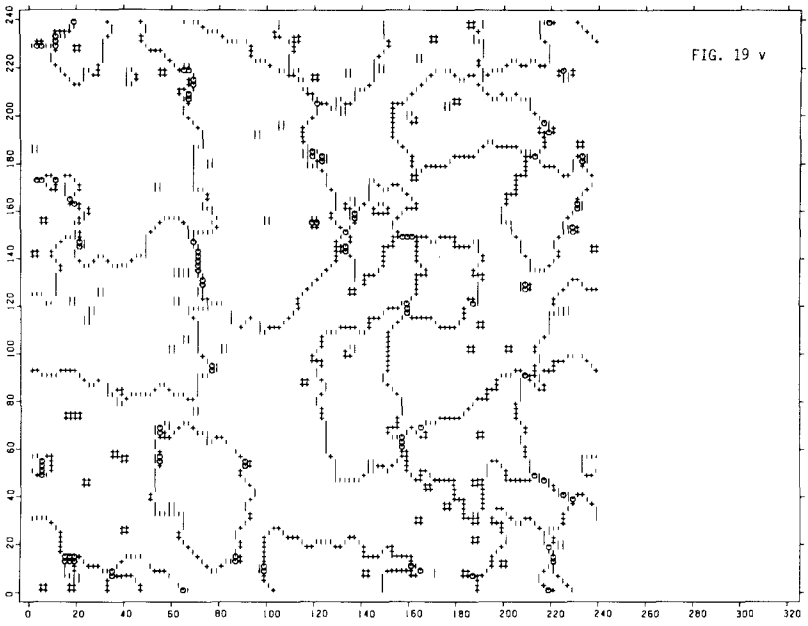

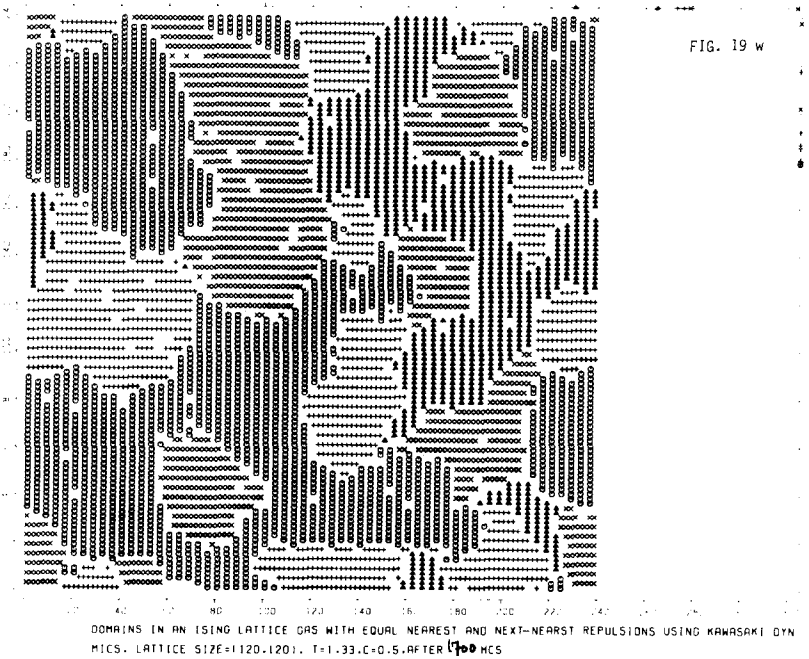

Fig. 19. Continued.

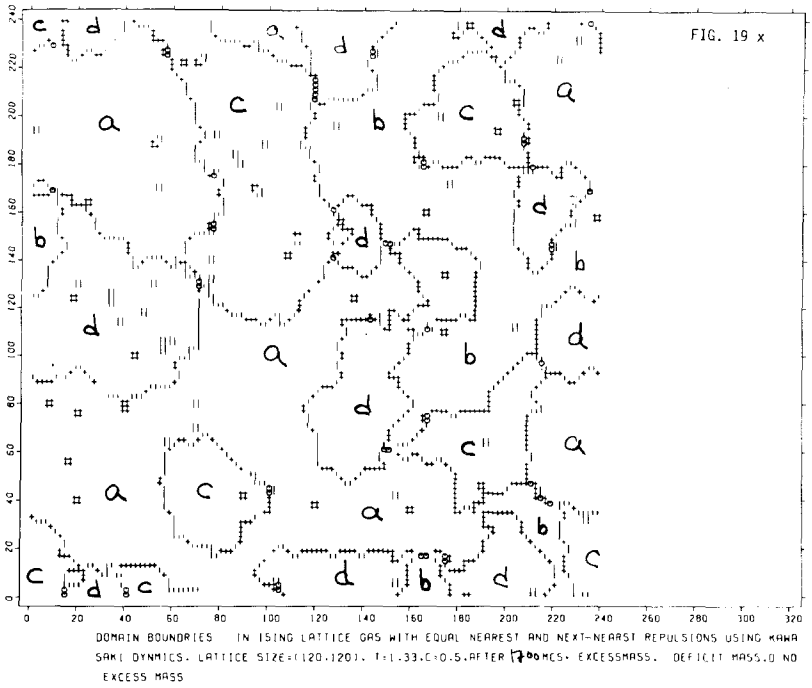

Fig. 19. Continued.

It then is natural to ask, why the conservation of density should make any difference and lead to even a significantly smaller value of the exponent x than in the case without conservation law. The answer to this question is simply that the density excess (or deficit, respectively) contained in the "heavy" or "light" walls needs to be redistributed by long-range diffusion, when the density is conserved, and some walls have to grow or shrink and finally disappear, or to diffuse as a whole, in order to allow for the growth of the domains. Clearly, the larger the domains become the smaller the gradients in the diffusion fields must become, similar as in the Lifshitz–Slyozov mechanism of coarsening in the late stages of phase separation.[39] Since in the latter case this slowing down of the diffusion controls the growth rate and leads to the law $L(t) \propto t^{1/3}$, we suspect that Eqs. (22), (23) really should be interpreted as $x = y = 1/3$ $(0 < T < T_c)$ for the present case as well.

In order to make these ideas more quantitative, we have studied the excess density (in spin terms, the excess magnetization Δm) in subsystem blocks of size $L_B \times L_B$, for L_B from 4 to 20, see, e.g., Fig. 20. It is seen that for smaller L_B the distribution sharpens up much more quickly than for

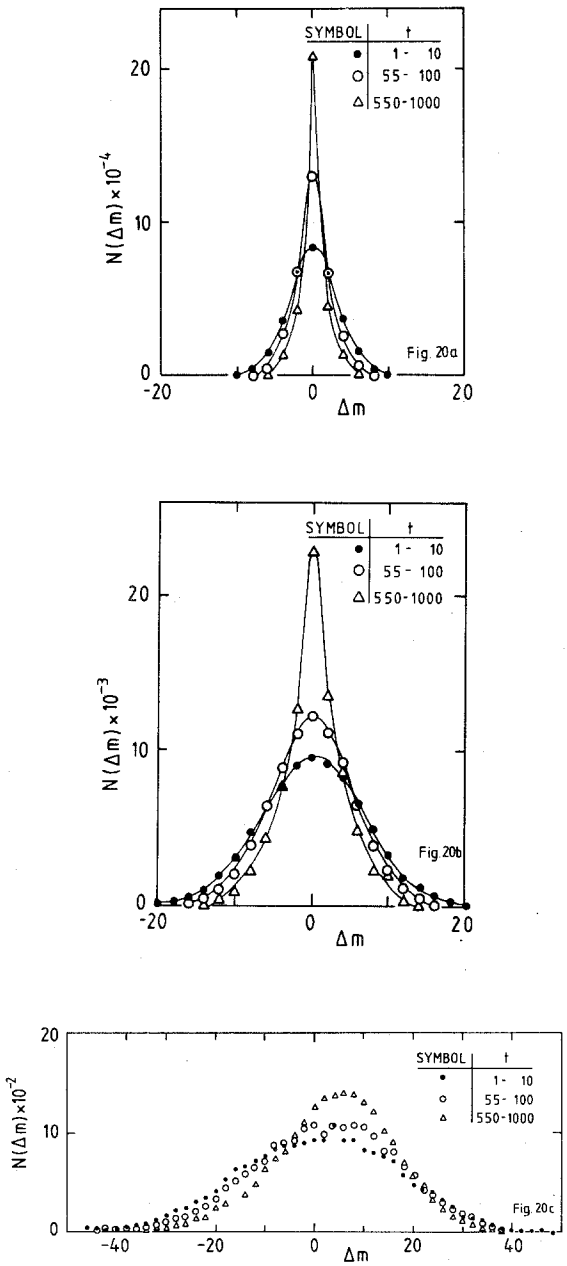

Fig. 20. Distribution of excess magnetization Δm in subsystem blocks of size 4×4 (a), 8×8 (b), and 16×16 (c), averaged over the time intervals as indicated in the figure. Data were taken for a 120×120 lattice at $T = 1.33$.

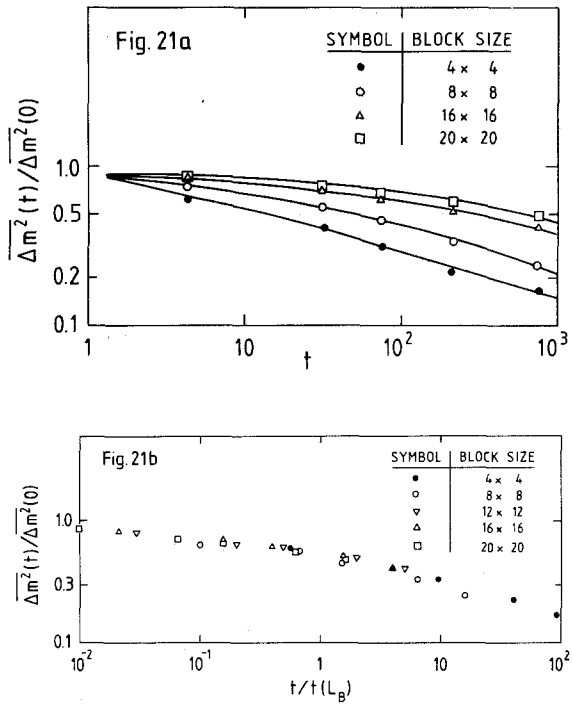

Fig. 21. Time evolution of the mean square density fluctuation $\overline{\Delta m^2(t)/\Delta m^2(0)}$ (a) and replotted in scaled form (b). The bars indicate time averaging (to smooth the data) over intervals as shown in Fig. 20.

larger L_B. This fact is seen more clearly in Fig. 21a, where the decrease of the relative width of these distributions is plotted vs. time. Defining a characteristic time $t(L_B)$ for each block size by

$$L\{t(L_B)\} \equiv L_B \tag{24}$$

we can find $t(L_B)$ immediately from Fig. 12a. Rescaling t with $t(L_B)$ one finds that now all curves $\overline{\Delta m^2(t)}/\overline{\Delta m^2(0)}$ superimpose on a single curve (Fig. 21b). This result is very gratifying: it directly shows that the time decay of the long wavelength density fluctuations is indeed coupled to the time evolution of $L(t)$, and in fact controls it!

5. QUENCHES LEADING TO $T = 0$ AND EVIDENCE FOR "GLASSY" STATES

Of course, the slowing down of the growth as T was lowered to 0.75, encountered in the previous section, makes one suspicious of what would

happen when one quenches the system to exactly $T = 0$. Figure 22 shows that then the growth of the domain size stops at about $L(t) \approx 10$, and also the decrease of the energy excess stops at about the same time ($t \approx 10^3$ MCS per particle). In order to check for possible logarithmic laws $L(t) \propto \ln t$,[11] we also plotted the energy excess versus this variable (Fig. 22b). It is seen that such a logarithmic law is not obeyed over any significant range of times. Unfortunately there seems to occur some systematic variation with finite size in our data, for which we do not have an explanation. Thus also our results for the structure factor in these quenches to $T = 0$ have to be taken with care (Fig. 23). It is quite remarkable, however, that the structure factor gets extremely broad wings. This shape of $S(q, \infty)$ is in

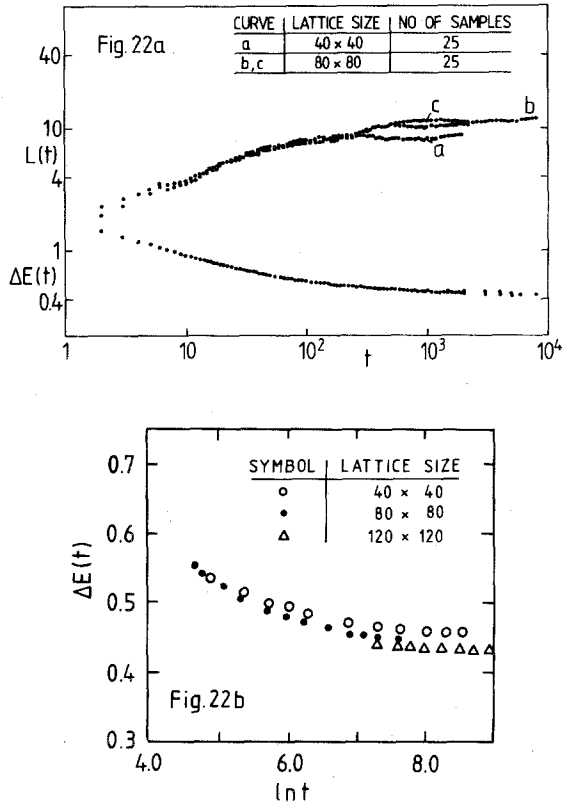

Fig. 22. (a) Log–log plot of $\Delta(t)$ and $L(t)$ vs. time, for the temperature $T = 0$ and conserved density $\rho = 1/2$. Lattice sizes and number of runs are indicated in the figure. (b) Energy excess plotted vs. $\ln t$ for three lattice sizes. (c) Snapshot picture of frozen domain configuration (same notation as in Fig. 19) at $t = 1200$ MCS.

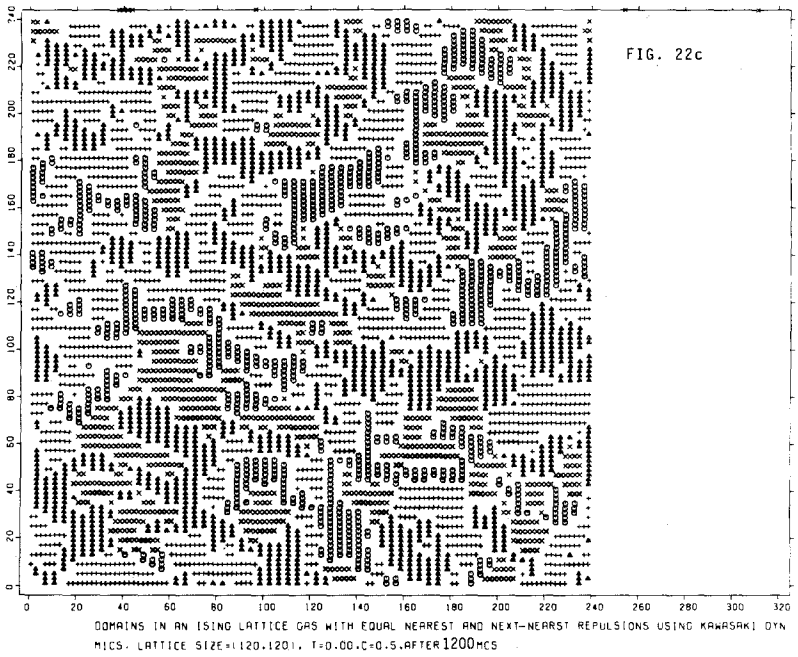

Fig. 22. Continued.

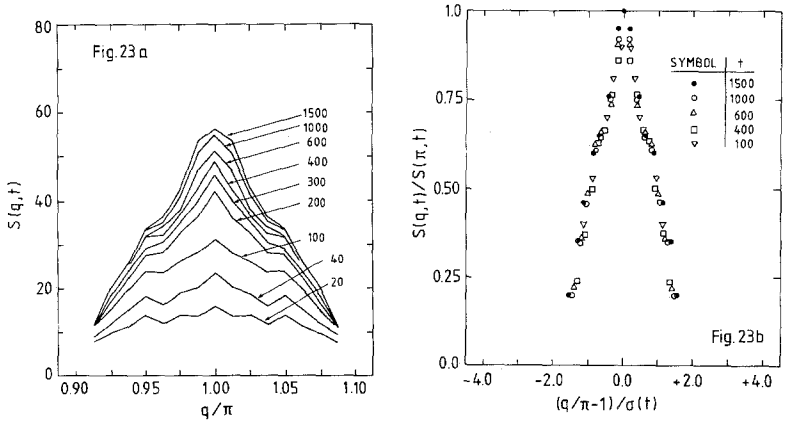

Fig. 23. Structure factor $S(q, t)$ plotted vs. q for various times after a quench to $T = 0$, for a 160×160 lattice (a, averages over 450 runs) and a scaling plot of the same data (b).

marked contrast to the scaled structure factor appearing in the late stages of finite temperature quenches (Fig. 17a).

Finally Fig. 22c exhibits typical pictures of the frozen-in glassy configurations.

6. SIMULATION OF QUENCHES INTO THE CRITICAL REGION

We first return to the case of single-spin flip dynamics (i.e., no conservation law). Figure 24 shows results for the time evolution of the energy excess and $L(t)$, which in this case is redefined as $L^2(t) \equiv [\psi_1^2(t) + \psi_2^2(t)]$. It is seen that the exponents x_c, y_c defined in analogy to Eq. (1)

$$L^2(t) \propto t^{2x_c}, \qquad E(t) - E(\infty) \propto t^{-y_c}, \qquad T = T_c \tag{25}$$

are no longer equal to each other: x_c is nearly temperature independent over the time interval shown, $x_c \approx 0.42$ at $T = 2.0$, $x_c \approx 0.34$ at $T \approx 2.1$ (not shown) and $x_c \approx 0.32$ at $T = 2.2$. In contrast, $y_c \approx 0.32$ at $T = 2.0$, $y_c \approx 0.40$ at $T \approx 2.1$ and between 0.5 and 1.0 at $T = 2.2$. The strong curvature of $\Delta E(t)$ on the log–log plot for $T = 2.2$ is qualitatively similar to the behavior at $T = 2.5$ (see Fig. 2(a)), i.e., it indicates crossover to an exponential decay which should occur for times t of the order of the equilibrium relaxation time τ,

$$\tau \propto \xi^z, \tag{26}$$

where $\xi \propto |1 - T/T_c|^{-\nu}$ is the order parameter correlation length, ν its

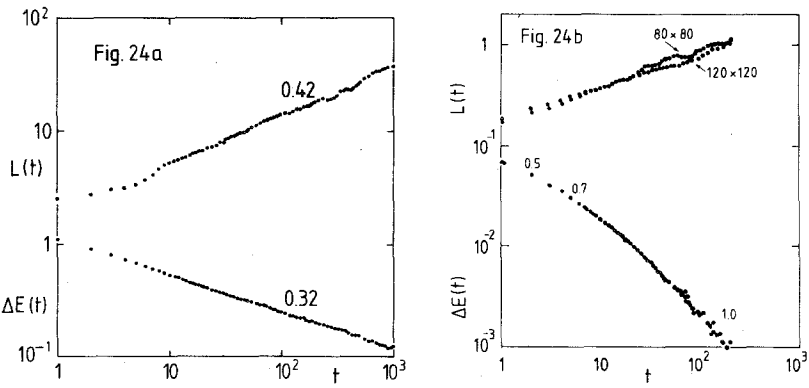

Fig. 24. Log–log plot of $L(t)$ and $\Delta E(t)$ vs. time for the model without conservation law at $H = 0$ ($\rho = 1/2$), $T = 2.0$ (a) and 2.2 (b). Numbers at the curves indicate effective exponents near the time where they are shown. Data are obtained from 80×80 and 120×120 lattices.

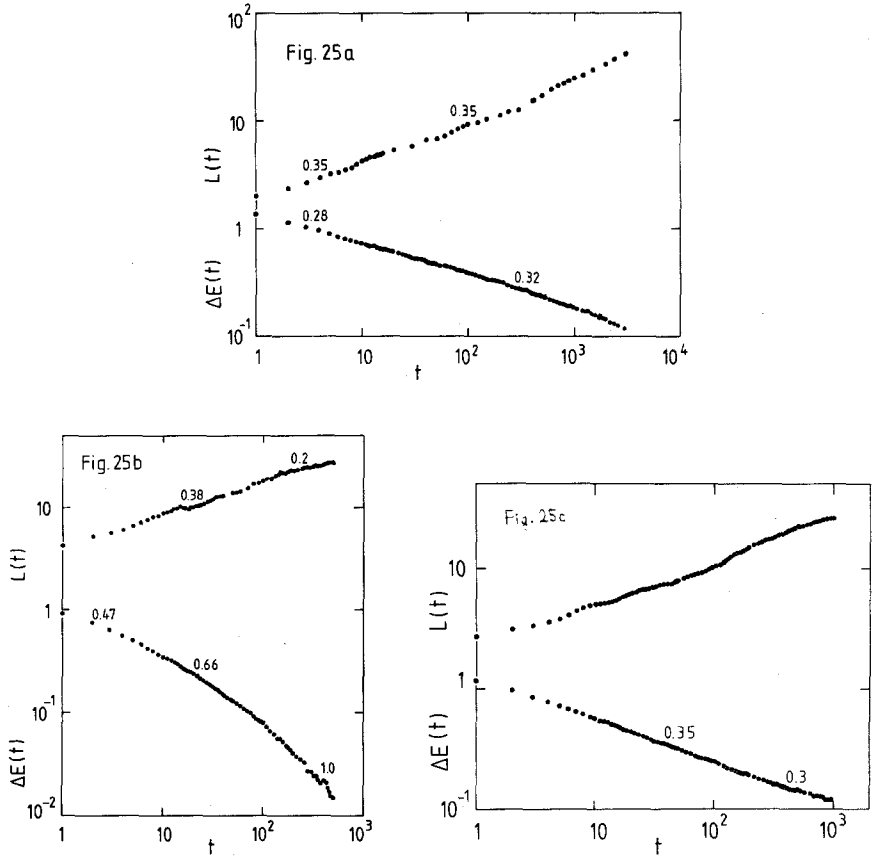

Fig. 25. Log–log plot of $L(t)$ and $\Delta E(t)$ vs. time for the model with conserved density at $\rho = 1/2$ and $T = 2.0$ (a), 2.2 (b), and 2.1 (c). Numbers at the curves indicate effective exponents near the time where they are shown. Data are obtained from 80×80 and 120×120 lattices.

critical exponent[28] and z is the dynamic critical exponent.[32] Similarly, we then expect that for $t \approx \tau$ in $L^2(t)$ a crossover sets in where $L^2(t)$ starts to saturate at its equilibrium value, the order parameter susceptibility χ_T which near T_c behaves as[28] $\chi_T \propto |1 - T/T_c|^{-\gamma} \propto \xi^{\gamma/\nu}$. This crossover can be expressed more quantitatively by postulating for $L(t)$ a dynamic scaling function[32,66]

$$L^2(t) = \xi^{\gamma/\nu} f(t/\tau) \equiv \xi^{\gamma/\nu} f_1(t\xi^{-z}) \tag{27}$$

where the function $f(u)$ {or $f_1(u)$, respectively} tends to a constant value for $u \to \infty$, in order that $L^2(t \to \infty)$ yields χ_T. On the other hand, at T_c $\xi = \infty$

and ξ then must cancel out from the expression Eq. (27), since $L(t)$ still is well defined and finite at T_c. This consideration hence yields that $f_1(u)$ for u small must behave as a power law, $f_1(u) \propto u^{2x_c}$, with

$$x_c = \gamma/2z\nu \tag{28}$$

Since the data for $T < T_c$ also show crossover at $t \approx \tau$ to the domain growth ruled by the exponent $x = 1/2$ found in Section 3, we conclude that the exponent x_c is probably in between the values found for $T = 2.0$ and 2.1, but closer to the latter,

$$x_c \approx 0.37 \pm 0.03 \tag{29}$$

Now the static exponents γ, ν of this model are nonuniversal, i.e., they depend on the ratio of interaction constants, magnetic field, etc.[31,49,50,67] For our case ($|J_{nn}| = |J_{nnn}|$, $H = 0$) they have been estimated by standard Monte Carlo finite-size-scaling analysis[49] as $\nu \approx 0.85$, $\gamma \approx 1.5$ and by Monte Carlo renormalization group[67] as $\nu = 0.87 \pm 0.02$ {asserting that $\gamma/\nu = 1.75$ is universal and has the same value as in the ordinary nearest-neighbor Ising model}. Hence Eqs. (28) and (29) yield immediately the estimate for the dynamic exponent z,

$$z \approx 2.4 \pm 0.2 \tag{30}$$

A similar reasoning can be presented for the excess energy, since the critical part of the energy scales as $|1 - T/T_c|^{1-\alpha} \propto (1 - \alpha)/\nu$, which is rewritten using the hyperscaling relation[28] $d\nu = 2\nu = 2 - \alpha$ as $|1 - T/T_c|^{1-\alpha} \propto \xi^{-2+1/\nu}$. The dynamic scaling law analogous to Eqs. (27) and (28) hence is found as

$$E(t) - E(\infty) = \xi^{-2+1/\nu} f_2(t\xi^{-z}) \tag{31}$$

where the function $f_2(u)$ must behave as $\ln f_2(u) \propto -u$ for $u \to \infty$, describing the exponential decay of the excess energy to zero, as found in Section 3. Since $E(t) - E(\infty)$ is finite and nonzero at T_c, the powers of ξ must then cancel in Eq. (31), which is only possible if $f_2(u) \propto u^{-y_c}$, with

$$y_c = (2 - 1/\nu)z \tag{32}$$

Concluding from our data that y_c should be in between the values found for $T = 2.0$ and 2.1, but probably closer to the minimum value found (any crossover effects should enhance rather than decrease y_c in this case), we suggest

$$y_c \approx 0.35 \pm 0.03 \tag{33}$$

Since $2 - 1/\nu \approx 0.85 \pm 0.03$, Eqs. (32) and (33) again lead to Eq. (30). This result that there is a unique exponent z for all relaxing quantities is known as "extended dynamic scaling."[32]

While the exponent $x = y = 1/2$ for $T < T_c$ both for the present model and the four-state Potts model,[17] the critical behavior of the two models renders them into different universality classes. The dynamic exponents z for the present model has not been studied before, while the estimates for z in the four-state Potts model lie in the range $2.5 \lesssim z \lesssim 2.7$.[68,69] Thus, with the accuracy presently available, it is not yet possible to clearly distinguish the dynamic universality classes! For better accuracy, much larger systems are necessary to avoid finite-size rounding, and to obtain better statistics. The recently developed special purpose–Monte Carlo processors[70] would be ideal for this purpose. Also experimental studies of critical dynamics of adsorbed layers via quenching experiments into the critical region would be desirable (other tools familiar from studies of three-dimensional systems, such as inelastic neutron scattering, hardly are applicable for adsorbed layers).

We next turn to critical quenches in the model with conserved density. The above considerations immediately carry over to the present case; only $f_2(u) \propto u^{-1}$ for large u, rather than decaying exponentially. Our numerical results are similar to the case without conservation: $x_c \approx 0.35$ at $T = 2.0$ and 2.1, while some crossover to saturation is seen at $T = 2.2$; similarly, $y_c \approx 0.32$ at $T = 2.0$, $y_c \approx 0.35$ to 0.30 at $T = 2.1$, while crossover to the $1/t$ relaxation characteristic for the disordered phase (Fig. 2) is seen at $T = 2.2$. Thus, we conclude

$$x_c \approx 0.35 \pm 0.03, \qquad y_c \approx 0.33 \pm 0.02 \tag{34}$$

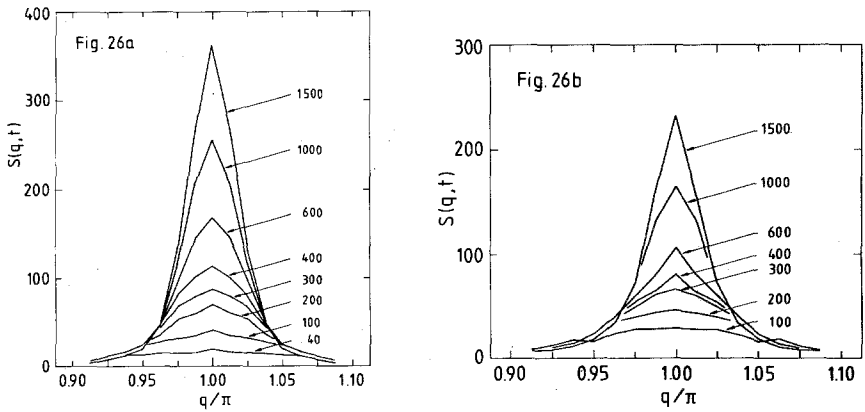

Fig. 26. Structure factor $S(q, t)$ plotted vs. q at $\rho = 1/2$ for the model with conserved density at $T = 2.0$ (a) and $T = 2.1$ (b), for a 160×160 lattice and averages over 250 runs at $T = 2.0$, 500 runs at $T = 2.1$. Numbers at the curves show the time t, measured in Monte Carlo steps per particle.

which yields as our estimate for the exponent z in the model with conservation law, from Eqs. (28), (32),

$$z \approx 2.55 \pm 0.15 \tag{35}$$

While the estimates Eqs. (30), (35) within their error bars overlap strongly, there is no reason to believe that they are exactly equal. In fact, according to the classification of universality classes[32] the present model belongs to class "C," while the model without any conservation belongs to class "A."

We also have obtained the structure factor $S(q,t)$ for the present model in the critical region (Fig. 26), and study its scaling properties in Figs. 27 and 28. Again scaling of $S(q,t)$ is well obeyed. A comparison with Fig. 17a reveals that the present scaling function $\tilde{S}(u)$ decays much slower in its wings. To interpret this behavior, we note that dynamic scaling in the critical region implies[32]

$$S(q,t) = \xi^{\gamma/2\nu}\hat{S}(k\xi, t\xi^{-z}) \tag{36a}$$

i.e., in the regime where $S(\pi,t)$ is far from saturation we have

$$S(q,t)/S(\pi,t) = (t\xi^{-z})^{\gamma/z\nu}\hat{S}(k\xi, t\xi^{-z}) \tag{36b}$$

Right at T_c the ξ factors must cancel out, implying that $\hat{S}(k\xi, t\xi^{-z}) \xrightarrow[\xi\to\infty]{} (t\xi^{-z})^{-\gamma/z\nu}\tilde{S}(kt^{1/z})$. Hence we find that the halfwidth $\sigma(t)$ of the structure factor must behave as

$$\sigma(t) \propto t^{-1/z}, \qquad T = T_c \tag{37a}$$

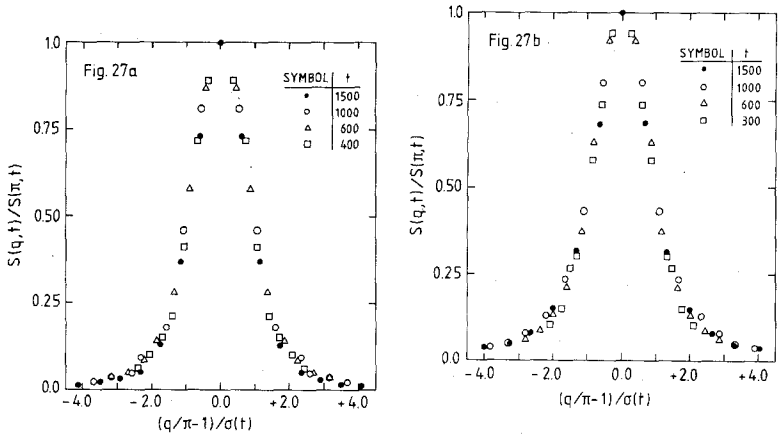

Fig. 27. Structure factor plotted in scaled form, normalizing $S(q,t)$ by its peak value $S(\pi,t)$ and $q/\pi - 1$ by the halfwidth $\sigma(t)$, for $T = 2.0$ (a) and $T = 2.1$ (b).

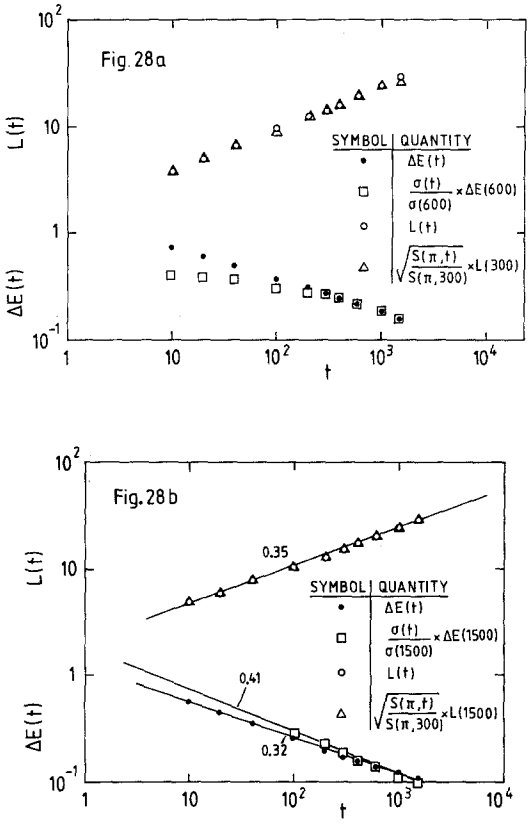

Fig. 28. Log–log plot of $L(t)$, $\Delta E(t)$, peak height $S(\pi, t)$ of the structure factor and its halfwidth $\sigma(t)$ plotted vs. time, for $T = 2.0$ (a) and $T = 2.1$ (b). Here $[S(\pi, t)]^{1/2}$ and $\sigma(t)$ are normalized such that they coincide with $L(t)$ or $\Delta E(t)$, respectively, at the times shown in the figure.

and $S(q, t)$ right at T_c scales as

$$S(q,t) = t^{\gamma/z\nu}\tilde{S}(kt^{1/z}) \tag{37b}$$

We emphasize that this result is no longer of the form of Eq. (2), since defining a length $l(t) = \sigma^{-1}(t) \propto t^z$ one rather gets $S(q, t) = [l(t)]^{\gamma/\nu}$ $\tilde{S}\{kl(t)\}$, the power $\gamma/\nu = 2 - \eta$ rather than the dimensionality d as in Eq. (2). Note that the quantity $L(t)$ is this section has no longer the dimension of a length and also does not play the role of a characteristic length, it is $l(t)$ which is the characteristic length of the problem. Unfortunately the data for $\sigma(t)$ at $T = 2.0$ exhibit much curvature, presumably due to cross-

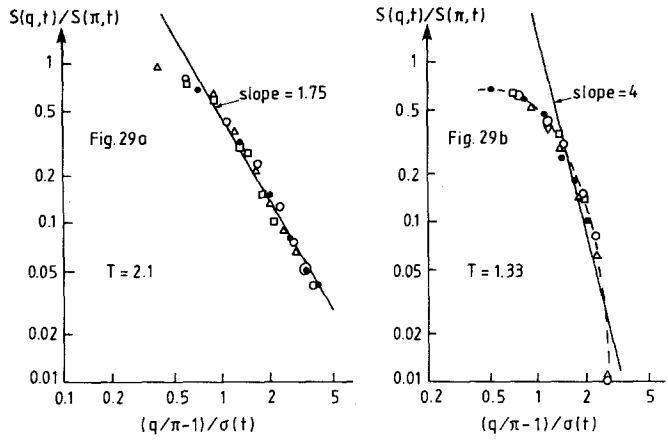

Fig. 29. Log–log plot of the scaled function $S(q,t)/S(\pi,t)$ vs. $(q/\pi - 1)/\sigma(t)$ at $T = 2.1$ and $T = 1.33$. The broken curve in the right part is only a guide to the eye.

over effects; but for $T = 2.1$ one can see that the exponent $1/z$ estimated from Eq. (37a) is $1/z \approx 0.41$, i.e., within our error estimates consistent with Eq. (35).

From the fact that $S(q,t)$ for $q \neq \pi$ should reach a finite limit at large times we immediately find, from Eq. (37b)

$$S(q \neq \pi, \infty) \propto k^{-\gamma/\nu} = k^{-(2-\eta)}, \qquad \tilde{S}(u) \underset{u\to\infty}{\propto} u^{-(2-\eta)} \tag{38}$$

Figure 29 shows that our data at $T = 2.1$ are indeed consistent with Eq. (38) $\{\eta = \frac{1}{4}\}$.[67] For comparison, the data for the scaling function of Fig. 17a at $T = 1.33$ are included: it is seen that the behavior is quite different, if one would try to fit a power law one would obtain a rather large exponent, of the order of 3–4 instead of 1.75. We do not have enough reliable data for $(a/\pi - 1)/\sigma(t) > 1$ to judge whether such a power law is a faithful representation of the scaling function $\tilde{S}(u)$ for large u. The prediction in the case $p = 2$ (and density not conserved) that[15] $\tilde{S}(u) \propto u^{-3}$ (for $d = 3$) is possibly also consistent with the present case.

7. DOMAIN WALL EXCESS DENSITY IN VARIOUS OTHER TWO-DIMENSIONAL STRUCTURES

In Section 4 we have seen that the conservation law for the density leads to domain growth exponents $x = y \cong 1/3$, rather than $x = y = 1/2$ as in the case without conservation law, and that the crucial point for this

change of exponents is the excess density contained in the domain walls. It is hence natural to ask, whether this mechanism is particular to the structure chosen, or whether it carries over to other cases as well.

First we consider the $c(\sqrt{2} \times \sqrt{2})$ structure, for which $p = 2$, and which has been studied in extensive previous work. Figure 30 shows that the domain walls oriented parallel to the lattice direction do *not* contain excess density. The "45° wall" would contain excess density, but it energetically clearly is unfavorable, and hence in the late stages such walls should not occur. Thus, we predict that the conservation law of the density should *not* affect the exponents x, y, as there is no excess density in the walls. This is consistent with theories {e.g., Ref. 6} and simulations {e.g., Refs. 10 and 20}.

The other structure with $p = 2$ is the $p(2 \times 1)$ structure; on a rectangular lattice it is reasonable to have interactions in the two lattice directions different from each other, and then the degeneracy between the two cases (a, b) and the two cases (c, d) in Fig. 1 is removed. The only important wall to consider is the "antiphase wall" of Fig. 7, which does not involve excess density as well. Hence again conservation of density should have no effect, and thus we predict $x = y = 1/2$ to apply, consistent with observation.[24]

The situation is quite different, however, for all cases with $p > 2$. Consider first the (3×1) structure on the centered rectangular lattice (Fig. 31). Depending on the interaction energies which stabilize this structure, it may be more favorable to have "antiphase boundaries" (Fig. 31a, b) or

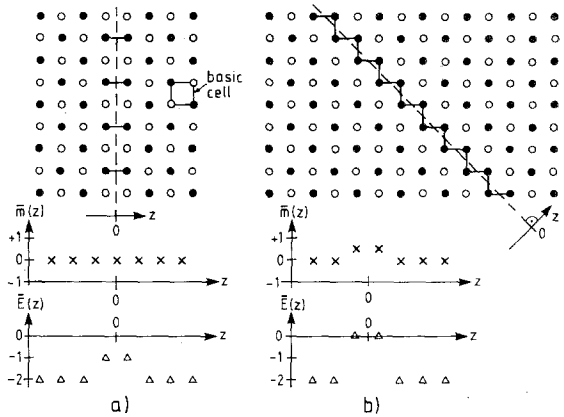

Fig. 30. "Antiphase boundary" (a) and "45° wall" (b) between the two types of ordered phases of the $c(\sqrt{2} \times \sqrt{2})$ structure. Underneath the arrangement of full and empty sites for each wall we display the profiles $\bar{m}(z)$ and $\bar{E}(z)$ of the magnetization and the energy, averaged along the wall, in the direction z perpendicular to the wall. Both cases refer to $T = 0$.

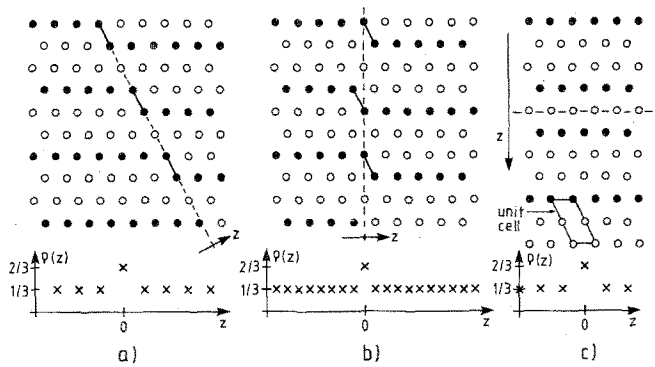

Fig. 31. "Antiphase boundary" (a, b) and "heavy wall" between domains of the (3×1) phase at density $\rho = 1/3$ on the centered rectangular lattice. Profile of the density $\rho(z)$ averaged in the direction parallel to the interface are also shown [in case (C) it is averaged over the unit cell shown].

"heavy walls" (Fig. 31c, in the case of density $\rho = 1/3$; for $\rho = 2/3$ the role of light and heavy is interchanged, of course). But now both types of walls exhibit excess density, and hence we predict that conservation of density should lead to domain growth exponents $x = y \cong 1/3$ as in the present study. It would be interesting to check this experimentally for the adsorption system H on Fe(110)[71] in which this structure has been observed. The situation is also similar for $(p \times 1)$ structures on this lattice with $p > 4$.

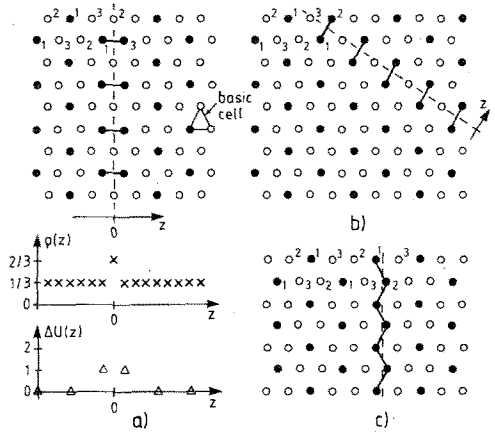

Fig. 32. Domain walls between ordered phases for the $\sqrt{3} \times \sqrt{3}$ structure on the triangular lattice (cf. text). The density profile $\rho(z)$ is averaged over the basic cell as indicated. Energy excess is measured in units of the nearest-neighbor energy.

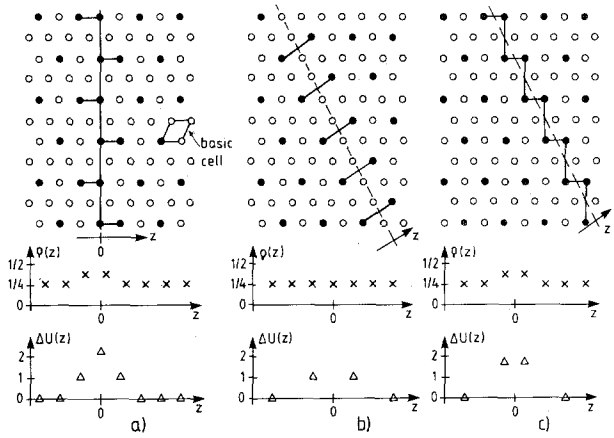

Fig. 33. Same as Fig. 32 but for the (2×2) lattice. Energy excess is only qualitative.

We now turn to the $\sqrt{3} \times \sqrt{3}$ structure on the triangular lattice, Fig. 32, which has $p = 3$ at $\rho = 1/3$ since then the sites of one of the three sublattices $1, 2, 3$ will be occupied, and the other two are empty. This structure already occurs if there is only a nearest-neighbor repulsive interaction on this lattice. Domain walls of the types a, b are energetically favorable, while the type c is unfavorable; but again every wall involves an excess density, and hence conservation of density should lead to $x = y \cong 1/3$ as the present study.

More complicated is the case of the (2×2) structure which may occur on the triangular lattice (Fig. 33) or square lattice at $\rho = 1/4$ or $\rho = 3/4$, respectively. In order to stabilize it on the triangular lattice, interactions up to at least next-nearest neighbors need to be included. Depending on the values of the interaction energies, it may be more favorable to have either "heavy walls" (a, c), which do involve excess density, or "antiphase boundaries" (Fig. 33b), which do not, at least in the ground state. It is conceivable, however, that at nonzero temperature these walls acquire excess density as well owing to the phenomenon of "interfacial adsorption" which has been shown to occur for $p > 2$ in various models.[72] Thus we conclude that the typical behavior of models with $p > 2$ with conserved density will be qualitatively similar to the results obtained in the present study, with $x = y \cong 1/3$ rather than $1/2$.

8. CONCLUSIONS

In this paper, extensive simulations of quenching experiments are reported, both for a model without any conservation law ("Glauber dynamics"), and a model with conserved density ("Kawasaki dynamics"); this

two-dimensional model undergoes a second-order transition from a disordered to a fourfold degenerate ordered state, and we consider quenches both to states within the disordered phase (leading to a state either above the transition or exactly at criticality) and to states within the ordered region (at nonzero as well as zero temperature). By carefully examining effects of finite size and of various crossover phenomena, we are able to sort out the asymptotic exponents governing the time evolution of the size of the growing domains (below T_c) or the susceptibility (above T_c), the excess energy and the structure factor.

While above T_c the approach to equilibrium of all considered quantities is exponential, apart from the excess energy in the case with conserved density which relaxes inversely proportional to the time after the quench, we find power laws for the relaxation right at T_c, which via dynamic scaling can all be related to a unique exponent z, with $z \approx 2.4 \pm 0.2$ (Glauber dynamics) and $z \approx 2.55 \pm 0.15$ (Kawasaki dynamics). Various evidences for the validity of dynamic scaling in both models is presented. Corresponding experimental studies in various chemisorbed monolayers at surfaces would be valuable.

Below T_c the domain size $L(t)$ behaves as $L(t) \propto t^x$, the halfwidth of the structure factor $\sigma(t) \propto t^{-x_\sigma}$, the excess energy with L^{-y}, where $x = x_\sigma = y = 1/2$ (Glauber dynamics) or $1/3$ (Kawasaki dynamics). The latter result is traced back to the excess density contained in the domain walls, which has to be redistributed over the scale $L(t)$ during the growth. A similar effect is predicted for various other ordered structures as well, provided their order parameter degeneracy $p \geqslant 3$. We find further that the structure factor can be expressed in scaled form.

Crossover effects near T_c (an in the conserved case also near $T = 0$) prevent us from checking whether the scaling function really is universal (as the domains near T_c are probably quite spherical and at low temperatures rather anisotropic, one might expect the scaling function to reflect this behavior and hence be temperature and density dependent). Finally we note that quenches to $T = 0$ in the conserved case freeze in a glasslike state with an irregular arrangement of very small domains.

ACKNOWLEDGMENT

One of us (K.B.) acknowledges support and hospitality of the Institute for Theoretical Physics, University of California—Santa Barbara, where a first draft of the manuscript was completed.

REFERENCES

1. I. M. Lifshitz, *Zh. Eksp. Teor. Fiz.* **42**:1354 (1962) [*Sov. Phys. JETP* **15**:939 (1962)].
2. M. Hillert, *Acta Met.* **13**:227 (1965).

3. N. P. Louat, *Acta Met.* **22**:721 (1974).
4. S. K. Chan, *J. Chem. Phys.* **67**:5755 (1977).
5. K. Kawasaki, M. C. Yalabik, and J. D. Gunton, *Phys. Rev. B* **17**:455 (1978).
6. S. M. Allen and J. W. Cahn, *Acta Met.* **27**:1085 (1979).
7. C. Billotet and K. Binder, *Z. Phys.* **B32**:195 (1979).
8. M. K. Phani, J. L. Lebowitz, M. H. Kalos, and O. Penrose, *Phys. Rev. Lett.* **45**:366 (1980).
9. P. S. Sahni and J. D. Gunton, *Phys. Rev. Lett.* **45**:369 (1980); **47**:1754 (1981).
10. P. S. Sahni, G. Dee, J. D. Gunton, M. K. Phani, J. L. Lebowitz, and M. H. Kalos, *Phys. Rev. B* **24**:410 (1981).
11. S. A. Safran, *Phys. Rev. Lett.* **46**:1581 (1981).
12. H. Furukawa, *Phys. Rev. A* **23**:1535 (1981); **28**:1717 (1983).
13. S. A. Safran, P. S. Sahni, and G. S. Grest, *Phys. Rev. B* **26**:466 (1982).
14. P. S. Sahni and G. S. Grest, *J. Appl. Phys.* **53**:8002 (1982).
15. T. Ohta, D. Jasnow, and K. Kawasaki, *Phys. Rev. Lett.* **49**:1223 (1982).
16. P. S. Sahni, G. S. Grest, and S. A. Safran, *Phys. Rev. Lett.* **50**:60 (1983); G. S. Grest, S. A. Safran, and P. S. Sahni, *J. Magn. Mag. Mat.* **31–34**:1011 (1983); S. A. Safran, P. S. Sahni, and G. S. Grest, *Phys. Rev. B* **28**:2693 (1983).
17. P. S. Sahni, G. S. Grest, M. P. Anderson, and D. J. Srolowitz, *Phys. Rev. Lett.* **50**:263 (1983); D. J. Srolowitz, M. P. Anderson, G. S. Grest, and P. S. Sahni, *Script Met.* **17**:241 (1983); P. S. Sahni, D. J. Srolowitz, G. S. Grest, M. P. Anderson, and S. A. Safran, *Phys. Rev. B* **28**:2705 (1983).
18. M. Grant and J. D. Gunton, *Phys. Rev. B* **28**:5496 (1983).
19. K. Kaski and J. D. Gunton, preprint.
20. K. Kaski, M. C. Yalabik, J. D. Gunton, and P. S. Sahni, preprint.
21. E. Burke and D. Turnbull, *Prog. Metal Phys.* **3**:220 (1952).
22. T. Hashimoto, T. Miyoshi, and M. Ohtsuka, *Phys. Rev. B* **13**:1119 (1976); T. Hashimoto, K. Nishimura, and Y. Takeuchi, *Phys. Lett.* **65A**:250 (1978); M. Sato and K. Mirakawa, *J. Phys. Soc. Japan* **42**:433 (1977).
23. M. G. Lagally, G. C. Wong, and T. M. Lu, *CRC Crit. Rev. Solid State Mat. Sci.* 7:233 (1978).
24. G.-C. Wang and T.-M. Lu, *Phys. Rev. Lett.* **50**:2014 (1983).
25. J. D. Gunton, M. San Miguel, and P. S. Sahni, in *Phase Transitions and Critical Phenomena*, Vol. 8, C. Domb and J. L. Lebowitz, eds. (Academic Press, London, 1983).
26. For a review, see J. S. Langer, *Rev. Mod. Phys.* **52**:1 (1980).
27. R. Bausch, V. Dohm, H. K. Janssen, and R. K. P. Zia, *Phys. Rev. Lett.* **47**:1837 (1981); see also K. Kawasaki and T. Ohta, *Prog. Theor. Phys.* **67**:147 (1982); **68**:129 (1982).
28. M. E. Fisher, *Rev. Mod. Phys.* **46**:587 (1974).
29. M. Schick, *Prog. Surf. Sci.* **11**:245 (1981).
30. F. Y. Wu, *Rev. Mod. Phys.* **54**:235 (1982).
31. S. Krinsky and D. Mukamel, *Phys. Rev. B* **16**:2313 (1977).
32. P. C. Hohenberg and B. I. Halperin, *Rev. Mod. Phys.* **49**:435 (1977).
33. K. Binder and D. Stauffer, *Phys. Rev. Lett.* **33**:1006 (1974); K. Binder, *Phys. Rev. B* **15**:4425 (1977).
34. K. Binder, C. Billotet, and P. Mirold, *Z. Phys.* **B30**:183 (1978).
35. J. Marro, J. Lebowitz, and M. H. Kalos, *Phys. Rev. Lett.* **43**:282 (1979); *Acta Met.* **30**:297 (1982); P. Fratzl, J. L. Lebowitz, J. Marro, and M. H. Kalos, *Acta Met.* **31**:1849 (1983).
36. P. S. Sahni and J. D. Gunton, *Phys. Rev. Lett.* **45**:369 (1980); P. S. Sahni, J. D. Gunton, S. L. Katz, and R. H. Timpe, *Phys. Rev. B* **25**:389 (1982); P. S. Sahni, S. L. Katz, and J. D. Gunton, preprint.

37. C. M. Knobler and N. C. Wong, *J. Chem. Phys.* **85**:1972 (1981); Y. C. Chu and W. I. Goldburg, *Phys. Rev. A* **23**:858 (1981).
38. A. Craievich and J. M. Sanchez, *Phys. Rev. Lett.* **47**:1308 (1981); M. Hermion, D. Ronzard, and P. Guyot, *Acta Met.* **30**:599 (1982); S. Komura, preprints.
39. I. M. Lifshitz and V. V. Slyozov, *J. Phys. Chem. Solids* **19**:35 (1961).
40. J. S. Langer, *Ann. Phys. (N.Y.)* **65**:53 (1971).
41. K. Tokuyama and K. Kawasaki, preprint.
42. K. Binder, *Solid State Commun.* **34**:191 (1980).
43. G. F. Mazenko and O. T. Valls, *Phys. Rev. Lett.* **51**:2044 (1983).
44. P. A. Rikvold and J. D. Gunton, *Phys. Rev. Lett.* **49**:286 (1982).
45. P. Fratzl *et al.*, Ref. 35, and Ref. 41.
46. K. Binder, *Phys. Rev. Lett.* **45**:811 (1980); *Z. Phys.* **B45**:61 (1981); K. Binder, M. H. Kalos, J. L. Lebowitz, and M. K. Phani, *Acta Met.* **29**:1655 (1981).
47. S. A. Safran, private communication.
48. H. Furukawa, preprint.
49. K. Binder and D. P. Landau, *Phys. Rev. B* **21**:1941 (1980).
50. K. Kaski, W. Kinzel, and J. D. Gunton, *Phys. Rev. B* **27**:6777 (1983).
51. P. A. Slotte, preprint.
52. D. P. Landau, A. Sadiq, and K. Binder, in preparation.
53. R. J. Glauber, *J. Math. Phys.* **4**:294 (1963).
54. K. Binder, ed., *Monte Carlo Methods in Statistical Physics* (Springer, Berlin, 1979); *Monte Carlo Methods in Statistical Physics II* (Springer, Berlin, 1983).
55. K. Kawasaki, in *Phase Transitions and Critical Phenomena* Vol. II, C. Domb and M. S. Green, eds. (Academic Press, New York, 1972).
56. E. Bauer, in *Phase Transitions in Surface Films*, J. G. Dash and J. Ruvalds, eds. (Plenum Press, New York, 1979), p. 267.
57. E. Bauer, private communication.
58. A. Sadiq and K. Binder, *Surf. Sci.* **128**:350 (1983).
59. A. Sadiq and K. Binder, *Phys. Rev. Lett.* **51**:674 (1983).
60. A. Sadiq, submitted to *J. Comp. Phys.*
61. A. B. Bortz, M. H. Kalos, and J. L. Lebowitz, *J. Comp. Phys.* **17**:10 (1981).
62. D. Stauffer, *Phys. Rep.* **54**:1 (1979).
63. L. van Hove, *Phys. Rev.* **93**:1374 (1954).
64. C. Billotet and K. Binder, *Physica* **103A**:99 (1980).
65. M. E. Fisher and Z. Racz, *Phys. Rev. B* **13**:5039 (1976).
66. R. Kretschmer, K. Binder, and D. Stauffer, *J. Stat. Phys.* **15**:267 (1976).
67. R. H. Swendsen and S. Krinsky, *Phys. Rev. Lett.* **43**:177 (1979).
68. K. Binder, *J. Stat. Phys.* **24**:69 (1981).
69. J. Tobochnik and A. Jayaprakash, *Phys. Rev. B* **25**:4891 (1982).
70. R. B. Peason, J. L. Richardson, and D. Toussaint, *J. Comp. Phys.* **51**:241 (1983); Hooghland, J. Spaa, B. Selman, and A. Compagner, *J. Comp. Phys.* **51**:250 (1983).
71. R. Imbihl, R. J. Behm, K. Christmann, G. Ertl, and T. Matsushima, *Surf. Sci.* **117**:257 (1982); W. Selke, W. Kinzel, and K. Binder, *Surf. Sci.* **125**:74 (1983).
72. W. Selke and W. Pesch, *Z. Physik* **B47**:335 (1982); W. Selke and D. A. Huse, *Z. Phys.* **B50**:113 (1983); W. Selke and J. Yeomans, *J. Phys.* **A16**:2789 (1983).